Canadian Science Publishing | Canadian Geotechnical Journal

Effect of Density on Skin Friction Response of Piles Embedded in Sand by Simple Shear Interface Tests

Journal:	*Canadian Geotechnical Journal*
Manuscript ID	cgj-2019-0243.R2
Manuscript Type:	Article
Date Submitted by the Author:	03-May-2020
Complete List of Authors:	Fakharian, Kazem; Amirkabir University of Technology, Civil & Environmental Engineering Vafaei, Nasrin; Amirkabir University of Technology, Civil & Environmental Engineering
Keyword:	Sand-pile interface, Non-displacement piles, Constant normal stiffness, Total tangential displacement, Shear deformation/Sliding displacement
Is the invited manuscript for consideration in a Special Issue? :	Not applicable (regular submission)

Effect of Density on Skin Friction Response of Piles Embedded in Sand by Simple Shear Interface Tests

Kazem Fakharian[a*] and Nasrin Vafaei[b]

[a] Associate Professor, Dept. of Civil & Environmental Engineering, Amirkabir University of Technology, Tehran, Iran

(kfakhari@aut.ac.ir, kfakhari@yahoo.com)

+98 (21) 6454 3003

+98 (21) 6641 4213 (fax)

[b] PhD Candidate, Dept. of Civil & Environmental Engineering, Amirkabir University of Technology, Tehran, Iran

(nasrin.vafaei@aut.ac.ir)

* Corresponding author.
E-mail address: kfakhari@aut.ac.ir

Abstract

This study focuses on a particular phenomenon related to the reduction in sand-pile skin friction with initial relative density increment from medium to dense. Frictional behaviour of sand-pile interface is simulated using a simple shear-type device capable of inducing constant normal stiffness condition. Sand-pile interface sliding and soil deformation components are distinguished quantitatively. The effects of initial relative density of sand, initial normal load, and constant normal stiffness are examined on the magnitude of the pile skin friction and shear displacement at failure. Results indicate that the magnitude of the mobilized shear stress at failure significantly relies on the shear stress state concerning the inflexion point on volume change graph, which is equivalent to the position of peak stress ratio. Good correlations exist between results of this study and field data of several heavily instrumented piles embedded in dense to very dense sands. The presented procedure is a useful framework for establishing more accurate skin friction calculation methodologies and t-z curve developments of axially loaded piles.

Keywords: Sand-pile interface, Non-displacement piles, Constant normal stiffness, Total tangential displacement, Shear deformation, Sliding displacement.

Introduction

The sand-pile interface zone controls the shear deformation and the ultimate shaft resistance of piles embedded in sand layers. Interface zone experiences large plastic simple shear mode strains (Fioravante 2002). Typically, the surrounding soil constrains any volume changes at the interface zone of a pile shaft (Fakharian 1996; Fakharian and Evgin 1997). When interface tests are carried out in the lab between sand and pile surface (steel or concrete), two factors are very significant, requiring special attention. They include “sliding displacement” between sand-plate and “volumetric compression/dilation” of the surrounding soil. The compression/dilation response can be simulated using a specific boundary condition normal to the contact surface known as “constant normal stiffness”. However, it should be noted that as the soil response to stress is nonlinear even at small magnitudes of strain, a constant normal stiffness may not adequately simulate the real response of the surrounding soil to normal displacement and normal stress variations. However, as simulation of variable normal stiffness is much more complicated, the constant normal stiffness has been used by researchers in several studies (e.g., DeJong and Westgate 2009; DeJong et al. 2003; Evgin and Fakharian 1998; Fakharian and Evgin 1997; Frost et al. 2004; Mortara et al. 2007; Poulos 1989; Randolph 2012). Moreover, the volumetric behavior of interface plays a substantial role in mobilized shear strength (Mortara et al. 2007; Wernick 1978). Therefore, the volumetric behavior of interface needs to be taken into account for evaluating the frictional response of piles embedded in sand.

Both direct shear and simple shear type interface apparatuses have been utilized by many researchers (e.g., Desai et al. 1985, DeJong and Westgate 2009; DeJong et al. 2003; Evgin and Fakharian 1998; Fakharian and Evgin 1997; Frost et al. 2004; Mortara et al. 2007; Poulos 1989; Randolph 2012). Initially, Uesugi and Kishida (1989, 1991) implemented a simple shear type box instead of the direct shear box. Subsequently, Fakharian and Evgin (1993, 1996) developed an apparatus capable of both direct shear and simple shear soil containers. They performed a series of direct shear and simple shear sand-steel plate interface tests. Comparing test results of the two soil containers indicated that peak and residual shear strengths from direct shear and simple shear boxes are almost identical. However, the simple shear box facilitates measuring and distinguishing the soil deformation and sliding displacement components (Fakharian and Evgin 1995). In other words, as far as the strength parameters of the interface are concerned, both direct shear and simple shear boxes are expected to result in similar magnitudes. However, for stiffness calculations and more detailed aspects of soil-structure frictional response, the simple shear method is preferred from the point of view of the authors. The advantages of simple shear box with respect to direct shear boxes become even more evident when cyclic loading is concerned, as pointed out in detail by Fakharian (1996) and Fakharian and Evgin (1995).

The load transfer (or t-z) method is one of the most widely used techniques in load-movement analysis of axially loaded piles. There are relations of shear stress between soil and pile skin on the pile shaft (denoted by t) and relative pile shaft movement at the same elevation (denoted by z) known as t-z curves in literature. The t-z method provides capability of modelling the reaction of soil surrounding the pile shaft using localized springs. Preferably, the nonlinear stress-strain behavior of soil should be incorporated into the t-z curves (Seidel and Coronel 2011). Recently, t-z curves obtained through accurate instrumentation and measurements on several pile shafts during axial loading of the pile in the field have provided valuable results on shaft resistance and response (Benzaria et al. 2013; Flynn and McCabe 2015; Puech 2013, Li et al. 2017). The t-z method provides a platform to model sand-pile frictional behavior through sand-steel/concrete element testing (Pra-ai and Boulon 2017; Randolph 2012).

All existing t-z approaches generally have parameters requiring to be determined by curve fitting of measured data obtained from field trial tests (Ni et al. 2017). But few projects can justify the high costs of the site specific and heavily-instrumented pile load tests. As a result, the design stage could rely primarily on laboratory test data such as principally constant normal stiffness (CNS) tests on sand-structural surface interface (Randolph 2012). In driven piles, stress condition severely changes during pile penetration (Lehane et al. 1993; Yang et al. 2013). Moreover, the surrounding soil undergoes volumetric and shear strains resulting in an increase of the adjacent soil density. An interface zone develops around the pile shaft consisting of fine broken soil particles (White and Bolton 2004). After pile installation, the density, particle size and stress state of adjacent soil significantly alter. Therefore, laboratory interface test data may not be applicable to account for the conditions of after pile installation around the pile shaft, unless the end-of-pile-installation conditions could adequately be simulated at the beginning of the interface shearing. As an alternative, the direct pile design methods based on cone penetration test (CPT) could be used to correlate the pile tip and shaft capacities to the penetrometer readings. In this research, a complete set of simple shear sand-steel plate interface tests are performed assuming the condition of a non-displacement pile embedded in sand subjected to monotonically increasing the axial load.

Fakharian and Evgin (1997) and Evgin and Fakharian (1996) performed “constant normal load” and “constant normal stiffness” tests on an interface between sand and a steel plate using a simple shear-type soil container. Their results showed that a considerable portion of the displacements due to shear deformation of sand took place before the peak shear strength was reached. After that, the shear deformation of sand mass was negligibly small while the sliding displacement at the contact surface continued. The sliding at sand-pile contact surface can be considered as the main reason of shear strength reduction and hence shear failure (DeJong and Westgate 2009; Fakharian and Evgin 1997; Mortara et al. 2007; Uesugi et al. 1988; Zhang and Zhang 2006).

Field observations revealing low magnitudes of frictional resistance of continuous flight auger, CFA, piles embedded in dense to very dense sands are reported (e.g., Puech 2013). Frictional resistance of the segments of the pile embedded in dense to the very dense zone is observed to be lower than those obtained from cone penetration results through the sand. Load transfer (t-z) curve results of Puech study showed that frictional resistance reduced by density increment from relatively dense (around 65%) to dense (D_r of around 80%). This specific observation was the main motive of the present study to further evaluate the mechanism of sand-pile interface frictional behaviour and the dependency of the frictional behaviour on the sand relative density. It is also of practical interest (in development of t-z relations) to find out the tangential displacement at which the shear failure occurs.

Adequate instruments such as strain gages are generally installed in piles to measure axial deformation (Krasinski and Wiszniewski 2017). The values of axial forces (Q_i) are deduced from pile shaft deformation measurements and Hooke's law ($Q_i = E_i\, \varepsilon_i\, A_i$, in which E_i , ε_i and A_i are elasticity or Young modulus, axial strain and pile cross section area of the pile in section 'i' of pile core, respectively). The deduced axial force is dependent on axial strain, Young modulus and cross-section area of the pile. The effect of reinforcement on Young modulus should be considered in reinforced concrete shafts. Additionally, in the case studies presented here, extensometers are also installed along the piles' shaft to directly measure the incremental displacements inferred as z component in produced t-z curves.

A comprehensive laboratory test program was planned to investigate a crushed silica sand–steel interface behaviour under different conditions. Simple shear interface tests with initial relative densities 30, 65 and 85% and initial normal stresses 50, 100, 200, and 300 kPa were performed under various magnitudes of constant normal stiffness (CNS). The simple shear interface test apparatus used is designed in such a way to accurately measure the "sliding displacement" between sand and steel plate that takes place during shearing of the interface. Additional tests were also performed using a ring shear apparatus equipped with piezoelectric bender elements followed by measuring the shear wave velocity for more precise characterization of the sand both under small and large strains.

Soil "shear deformation" and "sliding" at the sand-pile interface are evaluated and the state of stress and deformation/sliding at "phase transformation" and "peak stress ratio" are illustrated. The effects of initial relative density of sand, initial normal stress, and constant normal stiffness on the interface behaviour and soil deformability are evaluated and discussed. Furthermore, practical implications of this comprehensive experimental study are evaluated through comparisons between the interface test results of this study with interface behaviour measurements of Puech (2013) and Li et al. (2017) of several heavily instrumented piles embedded in sand and silty sand. The presented results could be further used for modifications of the pile skin friction resistance relations as well as t-z curve methodologies of non-displacement piles embedded in sand.

Simulation of Confining Pressure of Piles Embedded in Sand

As illustrated in Figure 1, the confinement effect from the far-field soil around the pile shaft can be simulated using linear springs perpendicular to the pile skin (Boulon and Forary 1986; Suriyavut Pra-ai and Boulon 2017). The simulated springs impose a normal stiffness condition onto the interface plane at any elevation between the pile shaft and the soil (Jardine et al. 2005). As a result, any alteration in the condition of the soil at the interface zone such as "compression" or "dilation" may cause a "decrease" or an "increase" in the magnitude of the normal stress acting on the interface, respectively (Fakharian 1996). Changes in the effective radial stress ($\Delta\sigma_n$) as a result of relative movement between pile shaft and soil tend to increase with the sand shear modulus and decrease with the pile diameter. Cavity expansion theory can then be used to define the far-field soil stiffness as shown in Equation 1 (DeJong et al. 2003; Jardine et al. 2005; Vesic 1972; Yu 2013):

$$K = \frac{\Delta\sigma_n}{\Delta v} = \frac{4G}{D} \quad (1)$$

where $\Delta\sigma_n$ is normal stress variation acting on the interface, Δv is normal displacement variation, G is surrounding soil shear modulus, and D is pile diameter.

For non-displacement piles without significant horizontal stress variations during the pile installation, initial radial stress σ_r is equivalent to the local free field horizontal effective stress. Therefore, the coefficient of lateral earth pressure at rest, K_0 could be used to estimate initial σ_r.

It is therefore rational to model the pile shaft shear stress-displacement and shear resistance through simple shear interface testing by applying a normal stress perpendicular to the interface plane (representing radial stress in the field) and a shear stress parallel with the interface plane (Figure 1). The normal boundary condition imposed by the surrounding soil is simulated through imposing a normal stiffness, K, on top of the testing box (Fakharian 1996; Fakharian and Evgin 1997; Shahrour et al. 2013; Pra-ai and Boulon 2016, 2017).

Materials and Test Methods

Soil and Pile Materials

The soil used in this research is crushed silica Firuzkuh sand (No. 131), supplied from Firuzkuh mine in the northeast of Tehran, Iran. It is generally a uniform silica sand (SP) with median grain size (D_{50}) of 0.71 mm, a specific gravity of 2.65, minimum and maximum void ratios of 0.642 and 0.919, respectively. The internal friction angles of sand are measured as 33.70, 35.04 and 36.10 degree, respectively, for 30, 65 and 85% relative densities, using direct shear test. Particle size distribution curve of this sand is plotted in Figure 2. The specific gravity is measured using ASTM D891-18. Minimum and maximum index densities are determined using ASTM D4254-16 and ASTM D4253-16, respectively.

To study the sand-steel interface response to shear loads, quite a few experiments were conducted on the interface between dry sand and a rough steel plate. An ST37 stainless steel plate is used, and sandblasting was employed to produce an average surface roughness (R_{max}) of 32.7 μm for a gauge length of (L_c) 0.8 mm. A sample surface profile of the ST37 steel plate is presented in Figure 3.

Relative roughness, R_n is generally used to normalize the structure surface roughness. It is using D_{50} of the soil grains at the contact surface and has been defined as $R_n = R_{\max}(L = D_{50}) / D_{50}$ (Kishida and Uesugi 1987). The individual particle interlocks with the structural surface at the largest individual heights (asperities) and depths of the surface profile along a distance equivalent to the particle length. Therefore, a gage length equivalent to the median size of particles, D_{50} is appropriate to measure R_{max} (maximum height to depth difference). The relative roughness, R_n is 0.05, representing the pile surface relative roughness. This magnitude is very important for two main reasons which are implicitly correlated. They are failure mode and the maximum mobilized interface friction angle (D'Aguiar et al. 2008). Besides, the coefficient of interface friction can be used to correct the surface roughness of the steel over a wide range of sand particle diameters (Kishida and Uesugi 1987). The normalized roughness coefficient is generally more than 0.05 for the typical pile surfaces such as oxidized mild steel or concrete (Randolph 2012). An average value of 5 surface roughness measurements along the interface shearing direction is reported as the value of R_{max}. The surface roughness parameters are determined from the surface profile as presented in Figure 3. The gage length (L_c = 0.8 mm) is selected almost close to the median grain size of the sand, which was 0.71 mm. The gauge length chosen (L_c = 0.8 mm) is the closest available value to the median grain size.

Skewness is defined as:

$$R_{sk} = \frac{1}{R_q^{\ 3}}\left[\frac{1}{L_c}\int_0^{L_c} Z^3(\mathrm{x})\,\mathrm{dx}\right] \tag{2}$$

where Z is individual heights (asperities) and depths of the surface profile. R_q is root-mean-square roughness, defined as:

$$R_q = \left[\frac{1}{L_c}\int_0^{L_c} Z^2(\mathrm{x})\,\mathrm{dx}\right] \tag{3}$$

The results of surface roughness parameters are shown in Table 1.

Recent studies on CFA piles have revealed a direct correlation between surface topography of pile with the type of surrounding soil. The surface roughness parameters of CFA pile surpass the comparative surface roughness parameters of a shot-blasted or a sand-blasted concrete (i.e., after artificial laboratory treatments). Among the available surface parameters, skewness is a parameter that controls surface friction. It has been reported that surface friction is higher for larger skewness values (Chen et al. 2019; Sedlaček et al. 2009, 2012). The measured skewness value for the surface of the CFA pile in contact with silty sand for three piles was measured as 0.1. The measured skewness value for the employed surface in this study is 0.085, indicating a surface having a friction even slightly lower than those reported for CFA piles surfaces embedded in similar strata. Therefore, the utilized roughness in the experiments presented in this study satisfactorily corresponds to the surface roughness of the target pile case study.

In the laboratory scale, shear wave velocity of the specimen (V_s) is measured using bender element (e.g., Alvarado and Coop 2012; Lee and Santamarina 2005; Viggiani and Atkinson 1995) and it is being calculated as shown in Equation 4:

$$V_s = \frac{d_{sr}}{t} \tag{4}$$

Where t is the travel time of the pulse and d_{sr} is the tip-to-tip distance between the source and receiver bender elements.

Vibrations generated by a bender element induce a small strain shear wave that propagates through the soil. The measured modulus at this low strain level is within the linear elastic domain and dependent on the confinement from the surrounding soil. Generally, V_s is related to the average stress on the polarization plane (σ'_0), and it can be defined as Equation (5) (Cha and Cho 2007; Hardin and Richart 1963; Lee and Stokoe 1986).

$$V_s = \sqrt{\frac{G_{\max}}{\rho}} = a\left(\frac{\sigma'_0}{1\ kPa}\right)^{\beta} \quad (5)$$

where G_{max} is the small-strain shear modulus. At σ_0 = 1 kPa, $a = V_s$. β shows the sensitivity of V_s to the state of stress.

The vertical stress was applied incrementally to both loose and dense specimens every 20 minutes. The magnitude of normal stress was varied between 50 to 900 kPa at increments of 50 kPa. Unloading stages were also included in the experiment; steps from 900 down to 100 kPa with 100 kPa decrements, every 20 minutes. In every step, the dial gauge readings and shear wave signals were recorded before the next loading step. The values of shear wave velocity and shear modulus with respect to vertical shears for three different relative densities 30, 65 and 85% are provided in Figure 4. It is observed that the calculated magnitudes using Equation 3 are in fair agreement with the measurements.

Simple Shear Apparatus

The sand-steel interface behaviour is tested using a fully-automated simple shear interface apparatus developed by Global-MTM. A picture of the Global MTM simple shear apparatus as well as an image of a sample are presented in Figure 5. The simple shear apparatus is capable of applying two orthogonal forces simultaneously, tangent and perpendicular to the interface plane to simulate shear (τ) and normal (σ_n) stresses in horizontal (x) and vertical (z) directions, respectively. The constant normal stiffness is maintained throughout the tests using a closed-loop computer-controlled system, ordering the servo system on z axes to adjust variations of normal stress with respect to normal displacement as a constant K. For more details, please refer to Fakharian (1996) and Fakharian and Evgin (1996, 1997). The soil container is a simple shear box with an interior area of 100 × 100 mm built using stacks of 2-mm-thick Teflon-coated, anodized, aluminum plates. A steel plate larger than the sand surface (150 × 200 mm) is used as the base for this simple shear box to keep the contact surface area constant during sliding. This configuration for interface tests is similar to those used by Uesugi and Kishida (1986) and Fakharian and Evgin (1997). To prevent leakage of the sand particles throughout shearing, a thin layer of polyurethane double-sided adhesive foam covered with a Teflon sheet is attached to the bottom surface of the lowest aluminum plate. As a result, no leakage of sand particles was observed during interface sliding.

Furthermore, differences between the sliding displacement along the contact surface and the displacement resulting from the shear deformation of the soil mass are distinguished using two linear variable differential transformers (LVDT). Figure 6 presents schematic diagrams of tangential displacements in the x-direction. The $LVDT\ a_x$ was used to measure the total tangential displacement (u_{xa}) between the top aluminum plate and the steel plate. Besides, the $LVDT\ b_x$ facilitates the measurement of the tangential displacement resulting from the shear deformation of the soil mass (u_{xb}) by reading the relative displacement between the top and bottom aluminum plates. Finally, the difference of total tangential displacement and the shear deformation of soil mass (u_{xa} - u_{xb}) is considered as the sliding displacement or slip across the soil-steel interface (u_x).

Sample Preparation Method

The specimens with 85% (very dense) and 65% (medium-dense) relative densities are prepared using multi-stage sieving pluviation method, with some modifications compared to Miuri and Toki (1982) and Fakharian and Evgin (1996). For preparing the interface test specimens with 30% relative density, dry sand is poured from a funnel positioned at a height of 150 mm as the funnel is shifted over the specimen chamber. The specimens in the simple shear container were 20 mm high for all the experiments.

Assumptions and Definitions

Soil Deformation and Sliding Ratios

Two new parameters, soil "deformation ratio" and "sliding ratio" are introduced to quantify the contribution ratios of "soil deformation" and "sliding displacement" components with respect to the "total tangential displacement", respectively. Soil deformation ratio and sliding ratio are defined as:

$$Soil\ Deformation\ Ratio = \frac{u_{xb}}{u_{xa}} \tag{6}$$

$$Sliding\ Ratio = \frac{u_{x}}{u_{xa}} \tag{7}$$

Phase Transformation and Inflection Points at the Interface

Phase transformation (PT) and inflexion points correspond to two specific stress states. The PT is a point at which the volume contraction changes to dilation during shear loading. The inflexion is a point to start a reduction of the rate of dilation, almost coinciding with the peak shear strength.

Results for test MD-100-K400 are presented in Figure 7 as a benchmark test. The sample was sheared to a total tangential displacement, u_{xa},, of 7 mm. Stress ratio and normal displacement variations during shearing are illustrated in Figures 7*a* and *b*, respectively. The PT points and peak stress ratios are depicted by circular and square marks, respectively, on all the graphs of Figure 7. Soil deformation and sliding ratios are shown in Figures 7*c* and *d*, respectively. As illustrated in Figure 7*c*, by arriving at PT point, rate of soil deformation has started to reduce slightly. The reduction in soil deformation corresponds to the onset of a slight increase in sliding displacement at the sand-steel contact surface, u_x (Figure 7*d*). Beyond the peak stress ratio point, however, soil deformation ratio has reduced significantly. Figure 7*d*, on the other hand shows that the sliding ratio has remarkably increased beyond the peak stress ratio point, indicating that the sliding propagation (slip) at the contact surface has taken over.

In summary, beyond the peak stress ratio, the interface has reached a state of sliding propagation, reduction in shear stress ratio, and failure commencement. Soil deformability and shear resistance at the pile-sand interface are correlated with several parameters such as the relative density of sand, initial normal load, normal stiffness boundary condition (representing confining pressure from the far-field surrounding soil in a direction normal to the pile shaft), and surface roughness of the pile shaft. The influences of the mentioned parameters above, are investigated in detail in the following sections.

Test Results and Evaluations

The details of the extensive monotonic testing program representing magnitudes of parameters and the loading condition for each test are summarized in Table 2. The required parameters are derived, assuming a non-displacement pile embedded in the sand. The *G* values are obtained from bender element test results, as shown in Figure 4. The magnitudes of normal stiffness and pile diameter are calculated using Equation 1. The assumptions and results are presented in the following subsections.

Effect of Relative Density on Interface Shear Strength

A very specific observation in the results of this study is the reduction of the mobilized shear stress between sand-steel (representing the pile skin friction resistance) at a relative density (D_r) of 85% compared to 65%. On the contrary, the mobilized shear stress at the D_r of 65% has increased compared to 30%. For example, according to Figures 8*a1*, *a2* and *a3*, by increasing initial D_r from 30 to 65%, the mobilized shear stress at 7 mm total shear displacement has risen substantially, which may be considered as a reasonable expectation. However, comparing the results with the same initial normal load and the same constant normal stiffness for 65% and 85% D_r shows that mobilized shear stresses for samples with 65% D_r are higher than those with 85% D_r for all K values. This observation may not be so well understood or acceptable in engineering practice. The questions here are if this observation could be actual and in particular, what are the reasons and practical implications? Repeating several of the tests showed precisely the same results. Moreover, similar trends are observed for different initial normal loads. The main issue to focus in this paper is further **interpretations** of the results as an attempt to find out the causes of the reduction of skin friction resistance with increase in relative density of sand.

Effect of Relative Density on Soil Deformability

Figures 8, 9 and 10 illustrate sand-steel interface test results for relative densities 30, 65, and 85% and constant normal stiffness (CNS) magnitudes 400, 700, 1200 and 2000 kPa/mm. All the 12 test results presented in Figures 8, 9 and 10 are having an initial normal stress of 100 kPa. As illustrated in Figures 8*a1*, *a2*, *a3* through 8*c1*, *c2*, *c3*, samples with higher D_r have represented lower shear deformation of soil (u_{xb}) and greater sliding displacement (u_x) at the sand-steel interface. For example, soil deformations at the total tangential displacement of 7 mm for CNS of 400 kN/mm and D_r 30, 65 and 85 percent are 5.79, 3.39 and 2.38 mm, respectively.

The PT and peak stress ratio lines are illustrated as threshold stress ratios through shear stress-normal stress space in Figures 9*a1*, *a2* and *a3*. The threshold stress ratios are also utilized to characterize PT and peak stress lines as shown in the stress ratio-tangential displacement spaces in Figures 9*b1*, *b2* and *b3* through *d1*, *d2* and *d3*. The corresponding points at which the PT line are touched, and the peak stress ratio line are un-touched are marked, respectively, by circular and square points. As illustrated in Figures 9*b1*, *b2* and *b3*, stress ratios have moved upward to reach the peak stress ratio lines. Further continuing the shearing, the stress path has approached the ultimate or critical state stress, which is more pronounced in dense samples. The point on peak stress ratio lines at which the stress path has reduced corresponds to "yield total tangential displacement" denoted by u_{xa-y}. To further clarify the definition of u_{xa-y}, its location corresponds to the total tangential displacement on peak stress ratio lines beyond which the sliding displacement at the sand-steel interface prevails. The definition of u_{xa-y} is useful in developing t-z relations in simulating the pile skin friction behaviour.

Relative density seems to be an essential factor influencing the magnitude of u_{xa-y}. According to Figures 9*c1*, *c2*, *c3*, *d1*, *d2* and *d3*, after reaching u_{xa-y} point, the sliding component prevails at the sand-steel contact surface. As shown in Figures 9*b1*, *b2* and *b3*, increasing in D_r of sand leads to a smaller total displacement mobilized to reach peak stress ratio lines and a shorter distance to follow up on the peak stress ratio line. In samples with D_r of 30%, stress ratio – total tangential displacement ($\tau / \sigma_n - u_{xa}$) paths have moved to reach at $(\tau / \sigma_n)_y$ and continued on peak stress ratio line (Figure 9*b1*) until total tangential displacement reached at u_{xa-y} and stress ratio started decreasing. The results show that the path with K of 2000 kPa/mm for the loose sample, has not reached the u_{xa-y} even at 7 mm total tangential displacement. In samples with D_r of 85%, however, $\tau/\sigma_n - u_{xa}$ curves have reached $(\tau / \sigma_n)_y$ and u_{xa-y} simultaneously, at the peak stress ratio, followed by an immediate stress ratio reduction (Figure 9*b3*).

The test results on very dense silica sand with D_r of 88% presented by Fakharian and Evgin (1997) had also indicated that during shearing of the sand-steel interface, most portion of shear deformation of sand took place before reaching the peak shear strength. After the peak shear strength, the shear deformation of the sand mass became negligibly small while the sliding displacement at the contact surface continued (Fakharian and Evgin 1997). In this study, however, a broader range of relative densities are attempted, and a framework is established to substantiate the shearing behaviour mechanism of sand-steel interfaces.

The magnitudes of yield stress ratios $(\tau / \sigma_n)_y$ for relative densities 30, 65 and 85% and various K are presented in Table 3. It is noticed that $(\tau / \sigma_n)_y$ is a function of relative density, varying from about 0.6 for loose samples to as high as 0.71 for very dense samples. The table also shows that with an increase in initial normal stress (σ_{n0}) and K, the yield stress ratio has slightly decreased.

Figure 11 illustrates the results of CNL sand-steel interface tests with initial relative densities 15, 30, 45, 60 and 88% under a constant normal stress of 100 kPa (with a surface roughness of 25 μm) carried out by Fakharian (1996). The results indicate that the peak stress ratios are considerably affected by D_r, ranging from 0.6 at 15% up to 0.8 at 88%. The residual stress ratios, however, are having the same magnitude of 0.62 for all the relative densities.

Shear Resistance of Piles

Effects of Initial Normal Load and Constant Normal Stiffness

Two factors are contributing to the shear resistance of pile shafts. They include pile-soil friction angle (the stress ratio in interface test results) and the magnitude of normal stress acting onto the interface plane. The pile frictional resistance (τ_f) is generally determined by the Coulomb failure criterion, on the basis of which the following relation is admitted to define the frictional resistance of piles embedded in granular soils:

$$\tau_f = \sigma_n \tan\delta = (\sigma_{n0} + \Delta\sigma_n)\tan\delta \qquad (8)$$

In Equation **8**, δ is the mobilized soil–pile interface friction angle. σ_n, σ_{n0}, and $\Delta\sigma_n$ are respectively, normal stress during shearing, initial normal stress, and the change in normal stress occurred because of soil–pile interface dilation or contraction. In fact, the dilation or contraction of the interface causes, respectively, increase or reduction in normal stress due to the confined boundary condition normal to the interface plane and proportional to the stiffness of the surrounding soil, denoted by K.

The variations of "soil deformation" and "sliding" ratios are illustrated with respect to total tangential displacement, u_{xa}, in Figures 10*a1*, *a2*, *a3* and 10*b1*, *b2*, *b3*, respectively. At the beginning of total tangential displacement increments until arriving to u_{xa-y}, the soil deformation ratio is indicated to be having a considerable value close to unity. The large value of soil deformation ratio is an indication that the soil deformation constitutes most of total tangential displacement. Thus, most of the shear resistance at the sand-pile interface is provided by the contribution of soil resistance. The soil deformation has resulted in an initial contractive response followed by a phase transformation and hence, dilative behaviour afterwards. The normal stress has also changed proportionally to the variations in normal displacement, which are shown to be in turn corresponding to the magnitudes of the normal stiffness and initial normal stress applied on the interface.

It is noticed from the figures that once reaching u_{xa-y}, the soil deformation ratio starts decreasing afterwards. The soil deformation ratio reduction is inversely proportional to the propagation of sliding at the sand-steel contact surface resulting in shear failure at the sand-steel interface. Afterwards, the stress ratio (τ/σ_n) decreases significantly approaching a residual state at which the total shear resistance is equivalent to the ultimate frictional resistance at the sand-steel contact surface.

Sand-steel interface friction angles are 32, 34.2 and 34.6 degree, respectively, for 30, 65 and 85% relative densities. On the other hand, the internal friction angles of sand were reported as 33.70, 35.04 and 36.10 degree, respectively, for 30, 65 and 85% relative densities, as pointed out in subsection of introducing soil and pile materials. Comparing the sand-steel interface friction angle with internal friction of sand, the interface friction angle is always smaller than internal friction angle in all the presented test results in this study. Therefore, the shear failure would have been expected to occur along the sand-steel interface, and not within the sand media. The deformation and sliding patterns of the stacks of rings containing the sand supports the expected deformation and sliding patterns. The results of Figures 10 comparing the variations of soil deformation ratio with respect to sliding displacement ratio before and after u_{xa-y} support the visual observations of the sliding plane at the sand-steel contact surface.

Effect of Relative Density

Figures 10*c1*, *c2*, *c3* and *d1*, *d2*, *d3* illustrate the normal displacement (same as volume change) and normal stress variations versus total tangential displacement, u_{xa}. Before reaching the inflexion point, at the same total tangential displacement and for the same normal stiffness, denser samples have shown a higher increase in normal stress resulted from a higher dilative response. After the inflexion point, however, it is surprisingly noticed that once comparing the results of 85% D_r to 65% D_r, lower normal stress and correspondingly, lower normal displacement are induced in the case of 85% D_r. The key reason is the fact that inflexion points of Figures 10c and *d* are stress states beyond which the dilatancy of the interface has tapered off. In other words, the potential of dilation (and hence increase in normal stress due to the effect of CNS boundary condition) remarkably has reduced beyond this inflexion point. Reconsidering Figures 9*b1*, *b2*, *b3*, clarifies that beyond inflexion point (almost peak strength), the stress ratios have decreased towards the residual strength. The corresponding mobilized shear stresses of Figures 8*a1*, *a2*, *a3* are correlated with the positions of inflexion points or peak strengths. By increasing the relative density, the inflexion points have moved backwards closer to PT point. Hence the normal displacements have a smaller chance to increase (Figures 10*d1*, *d2*, *d3*). The lack of sufficiently significant increases of normal displacements corresponds to lower mobilized shear stresses of dense samples.

The practical implication of this observation is that the mobilized shear stress between sand and pile skin does not necessarily keep increasing with D_r of sand. The variations of maximum mobilized shear stress with initial D_r for different CNS magnitudes, and initial normal stresses are plotted in Figure 12. The figure clearly indicates that the peak shear stresses have decreased from 65% to 85% D_r.

Therefore, a key point in estimating the magnitude of mobilized shear stress at any displacement is whether the shear displacement is beyond or before the inflexion point location. In other words, if the peak strength is already mobilized and the stress state is beyond the peak strength, then the rate of mobilized shear stress under CNS condition (which applies to the case of pile shaft resistance) reduces. As a result, lower shear resistances could be achieved for piles at higher relative densities. It is, therefore, essential knowing at different elevations on the pile shaft, the stress state is below or beyond the inflexion point (or peak strength), to calculate the shear resistance of the pile at that elevation.

Previous studies available on cyclic degradation of pile shaft resistance (e.g., Uesugi and Kishida 1986; Fakharian and Evgin 1997; DeJong et al. 2003) and friction fatigue in piling (Randolph 2012) have emphasized on the accumulation of sliding increments at interface zone and normal displacement amplitude diminishing by the number of cycles. Post-peak sliding propagations at sand-steel plate interfaces are reported in studies as mentioned above. Interfaces subjected to cyclic loads (or displacements) undergo successive compressive response at the interface zone. The monotonic shearing of the interface on the other hand, exhibits a low initial compression (until phase transformation, PT), followed by a dilative response afterwards. The governing rule of interface behaviour under both monotonic and cyclic loading is recognized to be the propagation of sliding displacement component at the sand-steel (or concrete) interfaces.

To further clarify and validate the applicability of the above findings from interface tests to the correlations of skin friction of piles with the relative density of sand, it is necessary to compare the results with field data. The next section presents the evaluation and interpretation of static load test results of two well-instrumented piles embedded in the sand. One is a CFA pile, and the other is a drilled shaft bored pile.

Validation with Field Data

Axial compressive static load test results on well-instrumented piles under different sand densities and pile diameters are required to validate the interface test results and findings presented in this study. However, field data are practically limited to specific sand density and pile diameter. Two well-documented projects having piles with extensive instrumentation embedded in sandy layers are selected as case studies from which the skin friction behaviour results are extracted and thoroughly evaluated and compared with the experimental results of this paper. Compressive loading test results performed on CFA (Continuous Flight Auger) piles belonging to the 'French National Project SOLCYP', are used for the verification purposes. Moreover, compressive loading test results performed on two drilled uncased bored piles presented by Li et al. (2017), are adopted for further evaluations.

The test site of the CFA pile is located at Loon-Plage near Dunkirk in northern France. The stratigraphy, cone penetration test (CPT) results and the sand relative density profile at Loon-Plage are presented in Figure 13. The water table at the time of pile testing was approximately 2 m below grade level. A silica sand layer exists between 2.2 and 11.5 meters of depth. The sand is fine (D_{50} = 0.15 mm) and poorly graded (uniformity coefficient C_U = 0.98). The average relative density between a depth of 4 to 8 m is about 80%. More details are presented in Benzaria et al. (2013) and Puech (2013).

The CFA Pile F4 (outer diameter OD = 420 mm, length L = 8 m) was instrumented with a set of LCPC removable extensometers. The t-z curves deduced from extensometers at different depths are shown in Figure 14. The details of the procedure to determine the local load transfer curves are presented in Benzaria et al. (2013). The t-z curves of the pile conceptually correspond to "shear stress-total tangential displacement" curves of Figures 8*a*1, *a*2 and *a*3 of the sand-steel interface. It would be, however, interesting to evaluate the results quantitatively to see how they compare to their corresponding interface test results.

One significant observation is the very low values of limit skin friction (τ_f < 45 kPa) obtained from the instrumented static load test. Puech (2013) has pointed out that "*ultimate skin frictions are low (in the range 20 kPa to 45 kPa) concerning the high values of cone resistance (10 to 30 MPa) and relative density (Dr ~ 80%)*".

Many correlations are available in the literature between the CPT tip resistance q_c, and pile tip and skin friction resistances (e.g. Bustamante and Gianeselli (LCPC method); De Kuiter and Beringen 1979, 1982; Eslami and Fellenius, 1997; Meyerhof 1956; Schmertmann 1978). Canadian Foundation Engineering Manual (CFEM, 2006) has proposed direct correlations between pile skin friction resistance and q_c, which is in fact, very similar to LCPC method, as shown in Equation 9:

$$\tau_f = \frac{1}{\alpha} q_c \qquad (9)$$

in which α is a coefficient depending on the pile type, installation method and soil type.

Focusing on the correlations between CPT test results and pile resistance, experimental data has shown that a good correlation exists between q_c and lateral (radial) stress in soil (Salgado et al. 1997; Salgado and Prezzi 2007). When a penetrometer is pushed into the soil, it creates and expands a cylindrical cavity. A rigid soil core with an approximately conical shape is formed under the base of the pile with an extending sloped line. In cross-section, soil beyond the pile base zone undergoes horizontal displacement (Salgado et al. 1997). The compression in surrounding soil resulted from horizontal displacement, mobilizes the utmost of radial stress and mobilized shear strength of the surrounding soil in q_c.

The magnitude of 1/α at peak strength of Pile F4 and also the proposed values from CFEM for the same pile type and sand density are illustrated in Figure 15*a*. It is noticed that the magnitude of 1/α has reduced with increasing q_c and reached to a strength independent ultimate value (1/α = 0.002) in very dense condition for Pile F4. But the magnitudes proposed by CFEM for 1/α are higher than those measured, and the differences have become more apparent with an increase in q_c, which is somewhat an indication of a higher density of sand. In other words, the skin friction obtained from CFEM is over-predicted at higher relative densities of sand.

To further evaluate the correlations between q_c and skin friction and sand density, the 1/α of peak stress ratios from the sand-steel interface tests are back-calculated and plotted in Figure 15*b*. Relation 10, as proposed by Salgado and Prezzi (2007) is used for estimating the equivalent q_c of the sand used in interface tests at different relative densities.

$$\frac{q_c}{p_a} = 1.64exp(0.1041\phi_c + (0.0264 - 0.0002\phi_c)D_r) * (\frac{\sigma'_h}{p_a})^{(0.841-0.0047Dr)} \qquad (10)$$

in which D_r is the sand relative density, ϕ_c is the critical-state friction angle, and P_a is a reference stress of 100 kPa. As shown in Figure 15*b*, 1/α has reduced by sand density and normal load increments and reached to a value of 0.0038 for 85% relative density and the (assumed) 447.8 mm pile of the test VD-100-K1200 (Table 2). The resulted 1/α values are reasonably close to each other for interface element testing results of this study and CFA Test Pile F4, which are 0.0038 and 0.002, respectively. Of course, the difference in 1/α values could be attributed to factors such as different sand types, surface roughness, etc., between Pile F4 and the interface test results of this study.

The presented results in Figures 15*a* and *b* indicate that there are reasonably good correlations between the back-calculated 1/α values for Pile F4 and interface element testing results of this study. However, the proposed 1/α values of CFEM have over-predicted the skin friction, in particular for dense sands of non-displacement piles. Pile F4 and interface element testing results have resulted in 1/α values in the range of 0.002 to 0.0044 for very dense samples. The 1/α predicted by CFEM, however, has resulted in a larger magnitude of 0.0067. CFEM proposes minimum amounts for 1/α, which is closer to the test condition, but still beyond the real quantities back-calculated from the field pile testing results.

The test site of the second case study, including two drilled uncased piles is located at the GEFRS in Corvallis, Oregon, USA. The soil layers and cone penetration test, CPT (SCPT) profiles of 4 experiments at GEFRS are presented in Figure 16. The water table at the time of pile testing was reported between 1.6 to 1.8 m below the grade level. There is a silty sand layer with 6.5 m thickness between 5.2 to 11.7 m. The mentioned layer consists of dense silty sand followed by gravel and intermittent seams of sandy silt. More details are presented in Li et al. (2017).

Two drilled uncased Piles MIR and HSIR (outer diameter OD = 915 mm, length L = 19.8 m) were fully instrumented. The instruments relevant for observing the axial load transfer included resistance strain gages installed on steel sister bars, concrete embedment vibrating wire strain gauges, load cells, dial gages and string-potentiometers. The surface of piles is reported as a rough contact surface as no long casing was used. Axial loads were applied to induce pile head displacements of 4.3 and 3.8 mm for piles MIR and SHIR, respectively. The measured, fitted and proposed t-z curves deduced from instrumentation at different depths are shown in Figure 17. Mark points show the measured values and dashed lines present the trends. The maximum measured t-z values are utilized for further calculations in this study. The details of the procedure to determine the local load transfer curves are presented in Li et al. (2017).

The magnitudes of 1/α corresponding to maximum measured strengths of Piles MIR, HSIR and also the proposed values in CFEM for the same pile types and sand densities are illustrated in Figure 18*a*. The same trend is observed similar to the previous case in that 1/α has reduced with increasing q_c and reached to an ultimate value of 0.00355 to 0.0057 in very dense condition. The comparisons show that at lower densities, CFEM has even under-predicted the tip resistance, while at very dense condition, the 1/α values are slightly over-predicted by CFEM. The results indicate that the differences are not very high compared to the former CFA pile case, but still, the significant reduction of 1/α with sand density is quite evident. Comparisons are then made for the 1/α corresponding to the maximum measured strength of Piles MIR, HSIR with those back-calculated from the results of this study. The comparisons show that the 1/α values of Piles MIR, HSIR are between the predicted values of this study. An exception is that the test piles have shown 1/α values higher than the results of this study at small values of q_c = 7.14 MPa, i.e. under loose sand condition.

It should be noted that there could be considerable discrepancies between the sand type, particle shape and size, pile surface roughness, etc., that affect the back-calculated 1/α values for the tested piles and interface test results. This is while the trends and even magnitudes satisfactorily compare to each other. However, more detailed studies comprised of both interface element testing as well as physical modelling and preferably, full-scale pile testing udder identical soil/surface and boundary conditions are required in future studies.

Discussion

In this study, the surface roughness investigated has been considered equivalent to that of an oxidized mild steel or a concrete surface to having simulated the prevailing pile surface conditions. However, the surface roughness has a significant controlling effect on shear stress-displacement (t-z) behaviour of the soil-pile interface. The results of interface tests with the same condition and different surface roughness, performed by Fakharian (1996) clarify the effect of surface roughness. The results of two CNL tests with the same normal stress and relative density of 100 kPa and 88%, respectively, but different surface roughness of 25 and 4 μm, presented by Fakharian (1996), are discussed here. The results indicate that the peak and residual shear stresses at rough surface condition are much higher than those in smooth surface, and the rough interface dilates significantly while the smooth interface contracts to reach a steady-state of stress.

Surface roughness also affects the loci of PT and peak stress ratio. Both PT and peak stress ratio have shifted to smaller total tangential displacements for smooth surface in comparison to rough surface.

Results of Subba et al. (1998) represent a nonlinear relation between increasing the ratio of interface friction angle to internal friction angle with relative roughness, R_n increment (Subba et al. 1998). Comparing the ratio of interface friction angle to internal friction angle for results of this study indicates δ/ϕ_p values of 0.94, 0.97 and 0.96 for samples with initial relative densities of 30, 65 and 85%, respectively. The proposed δ/ϕ_p value by Subba et al. (1998) at a relative roughness of (R_n =) 0.05 is 0.96. The R_n of the steel surface used in this study is also around 0.05. Therefore, the measured roughness values of this research are in good agreement with previous results.

It is noticed that surface roughness has a very significant effect on interface behaviour, shear strength and loci of PT and peak stress ratios. Further studies carrying out more number of experiments are required to focus on the influences of the magnitude of the surface roughness. In engineering practice, however, the real pile skins are usually having a surface roughness analogous to the implemented surface roughness in this study, as discussed in previous sections. Hence the results are expected to be valid for practical applications as far as the interface response of piles embedded in silica sand is concerned.

Conclusions

An attempt was made to simulate the sand-pile skin friction response (t-z) using simple shear interface tests under constant normal stiffness condition. Two new parameters, "soil deformation ratio" and "sliding ratio" are defined to determine the contribution levels of "soil deformation" and "sliding displacement" components versus the "total tangential displacement", resembling the axial movement of the pile with respect to the surrounding soil. Interface behaviour between sand-steel under different magnitudes of initial normal stress, sand relative density, and constant normal stiffness (*K*) was thoroughly examined. Special attention was paid on displacement and deformation characteristics at phase transformation (PT) and peak stress ratios. Results were compared with heavily instrumented field data of axially loaded piles. Based on the presented results, the most important findings of the study are summarized below:

1. Approaching the phase transformation point represents the onset of increasing the sliding displacement at the sand-steel interface as well as shifting the volume change response from contractive to dilative at the sand-steel interface.
2. Reaching the peak stress ratio point has resulted in prevailing the sliding displacement component, after which failure develops at the sand-pile contact surface. The point of inflexion on the volume change curve is equivalent to the peak

stress ratio, which is corresponding to the pile shear displacement at peak skin friction resistance.

3. The maximum mobilized shear stress under CNS condition could reduce with increase in relative density, if the inflexion point corresponding to peak stress ratio occurs at a low shear displacement level. The practical implication is that with an increase in relative density, shear resistance on the pile shaft may or may not increase, depending on the stress state with respect to the inflexion point.
4. The findings of the interface element test results at very dense condition were successfully validated by two axially loaded well-instrumented non-displacement test pile results. The results indicated that the proposed correlations between q_c of CPT test and skin friction of piles require modifications for dense sand conditions.
5. The loci of phase transformation and peak stress ratio are significantly affected by the surface roughness of the steel plate. The results seem to be valid, however, for representative surface roughness magnitudes of oxidized steel piles, CFA piles, and drilled shaft bored piles in engineering practice. Physical modelling and high-quality field test data are required, however, to further conclude the combined effects of the pile surface roughness and sand density.

Acknowledgments

The authors would like to acknowledge the technical and financial support of Global MTM for providing the testing facilities of this study. The contributions of Dr. Amirhossein Rezaie in facilitating the software and MTM mechanical engineers in developing the necessary components to simulate the constant normal stiffness condition is gratefully acknowledged. The authors would also recognize the contributions of Dr. A. Sadrekarimi at Western University, London, Ontario, in providing the ring shear device to perform the related experiments.

References

Alvarado, G., and Coop, M. R. 2012. On the performance of bender elements in triaxial tests. Géotechnique, 62(1): 1.

ASTM D891-18. Standard Test Methods for Specific Gravity, Apparent, of Liquid Industrial Chemicals, ASTM International, West Conshohocken, PA, 2018

ASTM D4254-16. Standard Test Methods for Minimum Index Density and Unit Weight of Soils and Calculation of Relative Density, ASTM International, West Conshohocken, PA, 2016

ASTM D4253-16. Standard Test Methods for Maximum Index Density and Unit Weight of Soils Using a Vibratory Table, ASTM International, West Conshohocken, PA, 2016

Bałachowski, L. 2006. Scale effect in shaft friction from the direct shear interface tests. Archives of Civil and Mechanical Engineering, 6(3): 13-28.

Benzaria, O., Puech, A., and Le Kouby, A. 2013. Essais cycliques axiaux sur des pieux forés dans des sables denses. Design for cyclic loading: Piles and other foundations. *In* Proceedings of TC 209 Workshop, 18th ICSMGE, Paris, pp. 73-76.

Boulon, M., and Foray P. 1986. Physical and numerical simulations of lateral shaft friction along offshore piles in sand. In: The 3rd international conference on numerical methods in offshore piling, Nantes, pp 127–147.

Brignoli, E. G., Gotti, M., and Stokoe, K. H. 1996. Measurement of shear waves in laboratory specimens by means of piezoelectric transducers. Geotechnical Testing Journal, 19(4): 384-397.

Bustamante, M., and Gianeselli, L. Pile bearing capacity prediction by means of static penetrometer CPT (LCPC method). *In* Proceedings of the 2-nd European symposium on penetration testing, pp. 493-500.

Cha, M., and Cho, G.-C. 2007. Shear strength estimation of sandy soils using shear wave velocity. Geotechnical Testing Journal, 30(6): 484-495.

Chen, L., Liu, Z., Wang, B., Song, Q., Wan, Y., and Chen, L. 2019. Surface Characterization and Tribological Performance of Anodizing Micro-Textured Aluminum-Silicon Alloys. Materials, 12(11): 1862.

D'Aguiar, S., Modaressi-Farahmand-Razavi, A., Lopez-Caballero, F., and Santos, J. 2008. Soil-structure interface modeling: Application to pile axial loading. *In* Proceedings of the 12th International Conference of the International Association for Computer Methods and Advances in Geomechanics (IACMAG), Goa, India, pp. 1-6.

DeJong, J. T., and Westgate, Z. J. 2009. Role of initial state, material properties, and confinement condition on local and global soil-structure interface behavior. Journal of Geotechnical and Geoenvironmental Engineering, 135(11): 1646-1660.

DeJong, J.T., Randolph, M.F., and White, D.J. 2003. Interface load transfer degradation during cyclic loading: a microscale investigation. Soils and Foundations, 43(4): 81-93.

De Kuiter, J., and Beringen, F. 1979. Pile foundations for large North Sea structures. Marine Georesources & Geotechnology, 3(3): 267-314.

Desai, C. S., Drumm, E. C., and Zaman, M. M. 1985. Cyclic testing and modeling of interfaces. ASCE, Journal of Geotechnical Engineering, 111(6): 793-815.

Dyvik, R., and Madshus, C. 1985. Lab Measurements of G_{max} Using Bender Elements. *In* Proceedings of Advances in the art of testing soils under cyclic conditions, ASCE, pp. 186-196.

Eslami, A., and Fellenius, B. H. 1997. Pile capacity by direct CPT and CPTu methods applied to 102 case histories. Canadian Geotechnical Journal, 34(6): 886-904.

Evgin, E., and Fakharian, K. 1997. Effect of stress paths on the behaviour of sand steel interfaces. Canadian Geotechnical Journal, 33(6): 853-865.

Evgin, E., and Fakharian, K. 1998. Cyclic rotational simple-shear behaviour of sand-steel interfaces. Soils and Foundations, 38(2): 191-199.

Fahey, M., Lehane, B., and Stewart, D. 2003. Soil stiffness for shallow foundation design in the Perth CBD. Australian Geomechanics, 38(3): 61-89.

Fakharian, K. and Evgin, E., 1993. A three-dimensional apparatus for cyclic testing of interfaces. Proceedings, 46th Annual Canadian Geotechnical Conference, Saskatoon, Canada, September 27-29, 1993, pp. 485-493.

Fakharian, K., and Evgin, E., 1995. Simple shear versus direct shear tests on interfaces during cyclic loading. In Proceedings of the 3rd International Conference on Recent Advances in Geotechnical

Earthquake Engineering & Soil Dynamics. 1995. Missouri S&T Library and Learning Resources, 1: pp. 13-16.

Fakharian, K. 1996. Three-dimensional monotonic and cyclic behaviour of sand-steel interfaces: Testing and modelling. Ph.D. dissertation, Department of Civil Engineering, University of Ottawa, Canada.

Fakharian, K., and Evgin, E., 1996. An automated apparatus for three-dimensional monotonic and cyclic testing of interfaces. Geotechnical Testing Journal, ASTM, GTJODJ, 19(1), 22-31.

Fakharian, K., and Evgin, E. 1996. An automated apparatus for three dimensional monotonic and cyclic testing of interfaces. Geotech. Testing J., ASTM, 19(1): 22-31.

Fakharian, K., and Evgin, E. 1997. Cyclic simple-shear behavior of sand-steel interfaces under constant normal stiffness condition. Journal of Geotechnical and Geoenvironmental Engineering, 123(12): 1096-1105.

Fioravante, V. 2002. On the shaft friction modelling of non-displacement piles in sand. Soils and Foundations, 42(2): 23-33.

Flynn, K.N., and McCabe, B. A. 2015. Shaft resistance of driven cast-in-situ piles in sand. Canadian Geotechnical Journal, 53(1): 49-59.

Frost, J.D., Hebeler, G.L., Evans, T.M., and DeJong, J.T. 2004. Interface behavior of granular soils. In Engineering, Construction, and Operations in Challenging Environments: Earth and Space 2004. pp. 65-72.

Hardin, B.O., and Richart Jr., F. 1963. Elastic wave velocities in granular soils. Proc. Journal of Soil Mechanics & Foundations Div, 89, 3407.

Jardine, R., Chow, F., Overy, R., and Standing, J. 2005. ICP design methods for driven piles in sands and clays, Thomas Telford London.

Kishida, H., and Uesugi, M. 1987. Tests of the interface between sand and steel in the simple shear apparatus. Geotechnique, 37(1): 45-52.

Krasinski, A., and Wiszniewski, M. 2017. Static load test on concrete pile–instrumentation and results interpretation.

Lee, J.-S., and Santamarina, J. C. 2005. Bender elements: performance and signal interpretation. Journal of Geotechnical and Geoenvironmental Engineering, 131(9): 1063-1070.

Lee, S. H., and Stokoe, K. H. 1986. Investigation of Low-Amplitude Shear Wave Velocity in Anisotropic Material. Texas University at Austin Geotechnical Engineering Center.

Lehane, B., Gaudin, C., and Schneider, J. 2005. Scale effects on tension capacity for rough piles buried in dense sand. Géotechnique, 55(10): 709-719.

Lehane, B.M., Jardine, R., Bond, A.J., and Frank, R. 1993. Mechanisms of shaft friction in sand from instrumented pile tests. Journal of Geotechnical Engineering, 119(1): 19-35.

Li, Q., Stuedlein, A., and Marinucci, A. 2017. Axial load transfer of drilled shaft foundations with and without steel casing. DFI Journal-The Journal of the Deep Foundations Institute, 11(1): 13-29.

Meyerhof, G. 1956. Penetration tests and bearing capacity of cohesionless soils. Journal of the Soil Mechanics and Foundations Division, 82(1): 1-19.

Miura, S., and Toki, S. 1982. A sample preparation method and its effect on static and cyclic deformation-strength properties of sand. Soils and Foundations, 22(1): 61-77.

Mortara, G., Mangiola, A., and Ghionna, V. N. 2007. Cyclic shear stress degradation and post-cyclic behaviour from sand–steel interface direct shear tests. Canadian Geotechnical Journal, 44(7): 739-752.

Ni, P., Song, L., Mei, G., and Zhao, Y. 2017. Generalized nonlinear softening load-transfer model for axially loaded piles. International Journal of Geomechanics, 17(8): 04017019.

Poulos, H.G. 1989. Cyclic axial loading analysis of piles in sand. Journal of Geotechnical Engineering, 115(6): 836-852.

Poulos, H., Carter, J., and Small, J. Foundations and retaining structures-Research and practice. In Proceedings of the International Conference on Soil Mechanics and Geotechnical Engineering. 2002. AA Balkema Publishers. pp. 2527-2606.

Pra-ai, S., and Boulon, M. 2016. Post-cyclic Behavior of Granular Soil-Structure Interface Direct Shear Tests. International Journal of GEOMATE, 11(24): 2328-2334.

Pra-ai, S., and Boulon, M. 2017. Soil–structure cyclic direct shear tests: a new interpretation of the direct shear experiment and its application to a series of cyclic tests. Acta Geotechnica, 12(1): 107-127.

Puech, A. 2013. Advances in axial cyclic pile design: contribution of the SOLCYP project. *In* Proceedings of TC 209 Workshop, 18 ICSMGE, pp. 1-17.

Randolph, M.F. 2012. Cyclic interface shearing in sand and cemented soils and application to axial response of piles. *In* Mechanical behaviour of soils under environmentally induced cyclic loads. *Edited by* C. Di Prisco, and D. M. Wood, eds. Springer Vienna, Vienna, pp. 481-528.

Salgado, R., Mitchell, J., and Jamiolkowski, M. 1997. Cavity expansion and penetration resistance in sand. Journal of Geotechnical and Geoenvironmental Engineering, 123(4): 344-354.

Salgado, R., and Prezzi, M. 2007. Computation of cavity expansion pressure and penetration resistance in sands. International Journal of Geomechanics, 7(4): 251-265.

Samanta, M., Punetha, P., and Sharma, M. 2018. Influence of surface texture on sand–steel interface strength response. Géotechnique Letters, 8(1): 40-48.

Schmertmann, J. 1978. Guidelines for cone test, performance, and design. Washington. DC Report FHWA-TS-78209, Federal Highway Administration.

Sedlaček, M., Podgornik, B., and Vižintin, J. 2009. Influence of surface preparation on roughness parameters, friction and wear. Wear, 266(3-4): 482-487.

Sedlaček, M., Podgornik, B., and Vižintin, J. 2012. Correlation between standard roughness parameters skewness and kurtosis and tribological behaviour of contact surfaces. Tribology International, 48: 102-112.

Seidel, M., and Coronel, M. C. 2011. A new approach for assessing offshore piles subjected to cyclic axial loading. Geotechnik, 34(4): 276-284.

Shahrour, M. I., Vincens, M. E., Emeriault, M. F., Canou, M. J., and Puech, M. A. 2013. Behaviour of soil-structure interfaces subjected to a large number of cycles. Application to piles. Ph.D. thesis, Department of Civil Engineering, Ecole Centrale de Lyon.

Subba, K., Allam, M., and Robinson, R. 1998. Interfacial friction between sands and solid surfaces. In Proceeding of the Institution if Civil Engineering: Geothechnical Engineering.

Uesugi, M., and Kishida, H. 1986. Frictional resistance at yield between dry sand and mild steel, Soils and Foundations, 26(4): 139-149.

Uesugi, M., Kishida, H., and Tsubakihara, Y. 1988. Behavior of sand particles in sand-steel friction. Soils and Foundations, 28(1): 107-118.

Uesugi, M., Kishida, H., and Tsubakihara, Y. 1989. Friction between sand and steel under repeated loading. Soils and Foundations, 29(3): 127-137.

Uesugi, M., and Kishida, H. 1991. Cyclic axial loading analysis of piles in sand. (Discussion), Journal of Geotechnical Engineering, ASCE, 115(6): 1435-1437.

Vesic, A.S. 1972. Expansion of cavities in infinite soil mass. Journal of Soil Mechanics & Foundations Div, 98(sm3).

Viggiani, G., and Atkinson, J. 1995. Interpretation of bender element tests. International Journal of Rock Mechanics and Mining Sciences and Geomechanics Abstracts, 8(32): 373A.

White, D., and Bolton, M. 2004. Displacement and strain paths during plane-strain model pile installation in sand. Géotechnique, 54(6): 375-397.

Wernick, E. 1978. Skin friction of cylindrical anchors in noncohesive soils. *In* Proceedings of Symp. on Soil Reinforcing and Stabilising Techniques, pp. 201-219.

Yang, Z., Jardine, R., Zhu, B., and Rimoy, S. 2013. Stresses developed around displacement piles penetration in sand. Journal of Geotechnical and Geoenvironmental Engineering, 140(3): 04013027.

Yu, H.-S. 2013. Cavity expansion methods in geomechanics, Springer Science & Business.

Zhang, G., and Zhang, J.-M. 2006. Monotonic and cyclic tests of interface between structure and gravelly soil. Soils and Foundations, 46(4): 505-518.

List of Symbols

The following symbols are used in this paper:

a = a variable

D = pile diameter

Dr = sand relative density

d_{st} = tip-to-tip distance between the source and receiver bender elements

G = soil shear modulus

G_{max} = small-strain shear modulus

K = constant normal stiffness

K_0 = coefficient of lateral earth pressure at rest

L_c = measurement length

P_a = reference stress of 100 kPa

q_c = CPT tip resistance

R_q = root mean-square roughness

R_{sk} = skewness

t = travel time of the pulse between tip-to-tip distance between the source and receiver bender elements

u_x = sliding displacement

u_{xa} = total tangential displacement

$u_{xa\text{-}y}$ = yield total tangential displacement

u_{xb} = shear deformation of the soil mass

v = normal displacement

V_s = shear wave velocity

z = depth

Z = individual heights (asperities) and depths of surface profile

α = a variable

β = a variable

$\Delta\sigma_n$ = normal stress variation acting on the interface

Δv = normal displacement variation

ϕ_c = critical-state friction angle

τ = shear stress

τ_f = pile frictional resistance

$(\tau/\sigma_n)_y$ = yield stress ratios

σ'_o = average stress on the polarization plane

σ'_h = horizontal effective stress

σ_n = normal stress during shearing

σ'_{n0} = consolidation normal stress

σ_{n0} = initial normal load

σ_r = radial stress

List of Figure Captions

Figure 1. Analogy between the localized shear stress along pile shaft and a simple shear test with an imposed normal stiffness (modified from Boulon and Forary 1986; Pra-ai and Boulon 2017).

Figure 2. Representative particle size distribution curve of Firuzkuh sand (131).

Figure 3. Surface profile of the ST37 steel plate used in this study.

Figure 4. Effect of normal stress and relative density, D_r on: (a) Shear wave velocity, (b) shear modulus of Firuzkuh sand (131).

Figure 5. Analogy between the localized shear along pile shaft and a simple shear test with an imposed normal stiffness (modified from Fakharian and Evgin 1997; Uesugi and Kishida 1986).

Figure 6. (a) Global MTM Simple shear apparatus, (b) An image of the sample, ready to start the test.

Figure 7. Positions of phase transformation (PT) and inflexion points for MD-100-K400 test.

Figure 8. Sand-steel interface test results with relative densities of 30, 65, 85%, 100 kPa initial normal stress, and 400, 700, 1200, 2000 kPa/mm constant normal stiffness.

Figure 9. Locations of PT and peak stress ratio points at stress space (a1-a3), stress ratio-total tangential displacement (b1-b3), stress ratio-shear deformation (c1-c3) and stress ratio-sliding displacement (d1-d3) for different relative density and *K* values.

Figure 10. More details of the sand-steel interface test results with relative densities of 30, 65, 85%, 100 kPa initial normal stress, and 400, 700, 1200, 2000 kPa/mm constant normal stiffness.

Figure 11. Comparisons between the results of CNL sand-steel interface tests with initial relative densities 15, 30, 45, 60 and 88% and initial normal load of 100 kPa (with surface roughness of 25 μm) (Fakharian 1996).

Figure 12. Peak shear stress, τ_y varaition with relative density, for normal stifnesses of 400, 700, 1200 and 2000 kPa/mm.

Figure 13. Soil layering and CPT profiles at Loon-Plage (modified from Benzaria et al. 2013).

Figure 14. Local shear transfer (t-z) curves in Flanders sand from static load test on CFA pile F4 at different depths (modified from Benzaria et al. 2013).

Figure 15. Magnitudes of 1/α for: (a) peak shear strength obtained from mesured t-z curves and proposed values of CFEM for Pile F4, and (b) peak stress ratio for sand-steel interface tests and proposed values of CFEM for 30, 65 and 85% relative densities.

Figure 16. Soil layering and CPT profiles at GEFRS site (modified from Li et al. 2017).

Figure 17. Measured, fitted and proposed t-z responses for the two uncased test pile (a) HSIR and (b) MIR for load increments from 5.5 to 7.9 m (18–26 ft) (modified from Li et al. 2017).

Figure 18. magnitudes of 1/α for: (a) mesured values obtained from deduced t-z curves and proposed values of CFEM for Piles MIR and HSIR, and (b) comparing peak stress ratio for sand-steel interface tests and obtained values for Piles MIR and HSIR.

Table 1. Results of the measurements of roughness parameters for surface profile of the sand blasted ST37 steel plate used in this study.

Name of parameter	unit	Measured value
Average roughness (R_a)	(μm)	5.0
Average of all $R_{max}s$ (R_z)	(μm)	32.7
root mean-square roughness (R_q)	(μm)	6.4
Skewness (R_{sk})	-	0.085

Table 2. Outline of tests and parameters

Test Identification[*]	$\sigma'_h = \sigma_{n0}$ (kPa)	K (kPa/mm)	G_{max} (kPa)	D (mm)	Z (m)	Dr %	q_c (MPa)
L-50-K400	50	400	60530	605.3	5.3	30	5.82
L-50-K700		700		345.9			
L-50-K1200		1200		201.8			
L-50-K2000		2000		121.1			
L-100-K400	100	400	73950	739.5	10.7	30	9.45
L-100-K700		700		422.6			
L-100-K1200		1200		246.5			
L-100-K2000		2000		147.9			
L-200-K400	200	400	86870	868.7	21.3	30	15.35
L-200-K700		700		496.4			
L-200-K1200		1200		289.6			
L-200-K2000		2000		173.7			
MD-50-K400	50	400	94150	941.5	3.4	65	13.85
MD-50-K700		700		538			
MD-50-K1200		1200		313.8			
MD-50-K2000		2000		188.3			
MD-100-K400	100	400	115200	1152	6.8	65	20.09
MD-100-K700		700		658.3			
MD-100-K1200		1200		384			
MD-100-K2000		2000		230.4			
MD-200-K400	200	400	132120	1321.2	13.5	65	29.11
MD-200-K700		700		755.0			
MD-200-K1200		1200		440.4			
MD-200-K2000		2000		264.2			
VD-50-K400	50	400	112828	1128.3	5.4	85	22.39
VD-50-K700		700		644.7			
VD-50-K1200		1200		376.1			
VD-50-K2000		2000		225.7			
VD-100-K400	100	400	134330	1343.3	5.4	85	22.39

VD-100-K700		700		767.6			
VD-100-K1200		1200		447.8			
VD-100-K2000		2000		268.7			
VD-200-K400	200	400	150880	1508.8	10.8	85	30.41
VD-200-K700		700		862.2			
VD-200-K1200		1200		502.9			
VD-200-K2000		2000		301.8			
VD-300-K400	300	400	176150	1761.5	16.3	85	41.30
VD-300-K700		700		1006.6			
VD-300-K1200		1200		587.2			
VD-300-K2000		2000		352.3			

Note: * Density-initial normal load-constant normal stiffness, $K_0 = 1 - \sin(\varphi') + (\gamma_d/\gamma_{d(min)}-1)5.5$; L, MD and VD in test labels indicate loose, medium dense and very dense samples; σ'_h = horizontal stress; σ'_{n0} = consolidation normal stress; K = normal stiffness; G_{max} = max shear modulus; D = pile diameter; Z = depth; Dr = consolidation relative density; q_c = CPT tip resistance.

Table 3. Magnitudes of "peak stress ratio" resulted ffrom different tests

σ_{n0} (kPa)	K (kPa/mm)	Dr →	$(\tau/\sigma_n)_y$ 30%	65%	85%
50	400		0.641	0.702	0.710
100			0.622	0.685	0.690
200			0.607	0.677	0.678
300					0.677
50	700		0.642	0.689	0.69
100			0.621	0.655	0.685
200			0.607	0.669	0.678
300					0.679
50	1200		0.634	0.681	0.695
100			0.626	0.68	0.691
200			0.604	0.662	0.681
300					0.679
50	2000		0.631	0.688	0.685
100			0.621	0.687	0.682
200			0.602	0.679	0.676
300					0.669

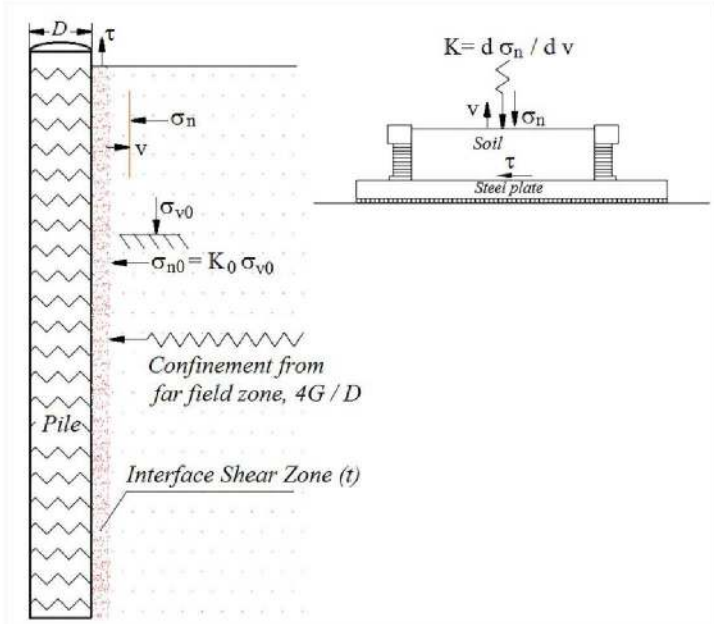

Figure 1. Analogy between the localized shear stress along pile shaft and a simple shear test with an imposed normal stiffness (modified from Boulon and Forary 1986; Pra-ai and Boulon 2017).

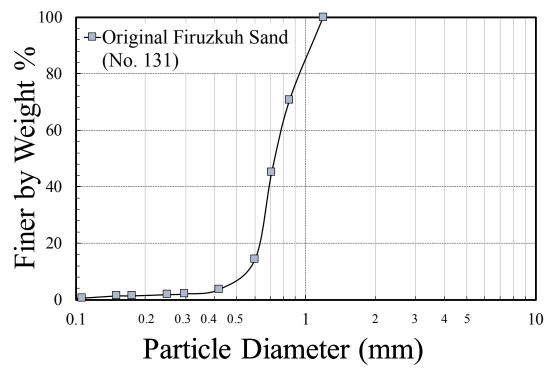

Figure 2. Representative particle size distribution curve of Firuzkuh sand (131).

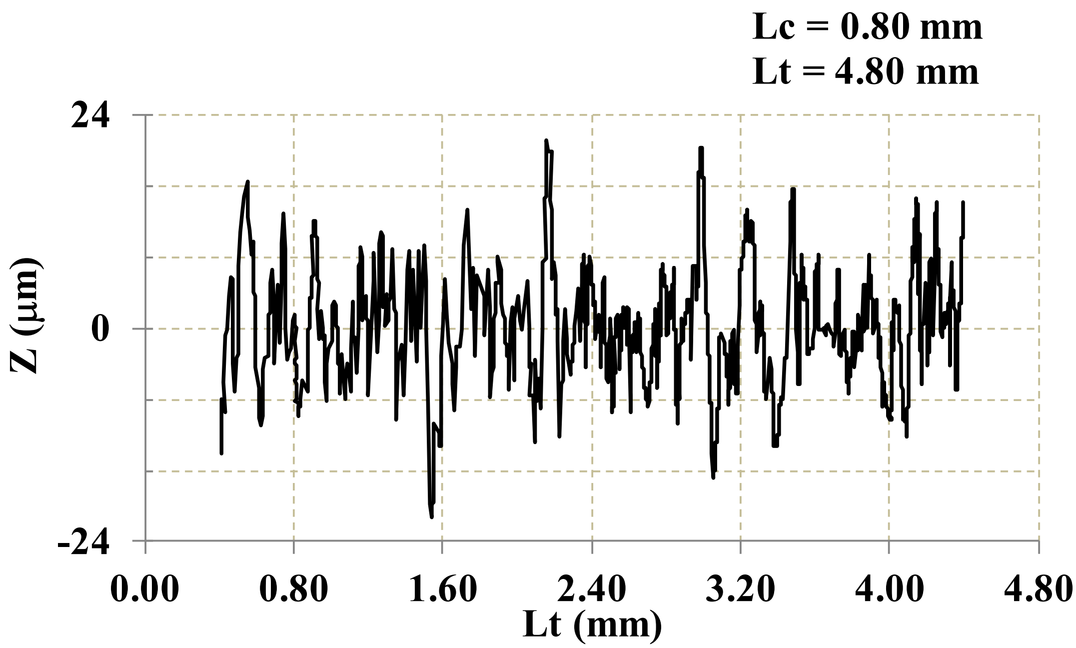

Figure 3. Representative surface profile of the ST37 steel plate used in this study.

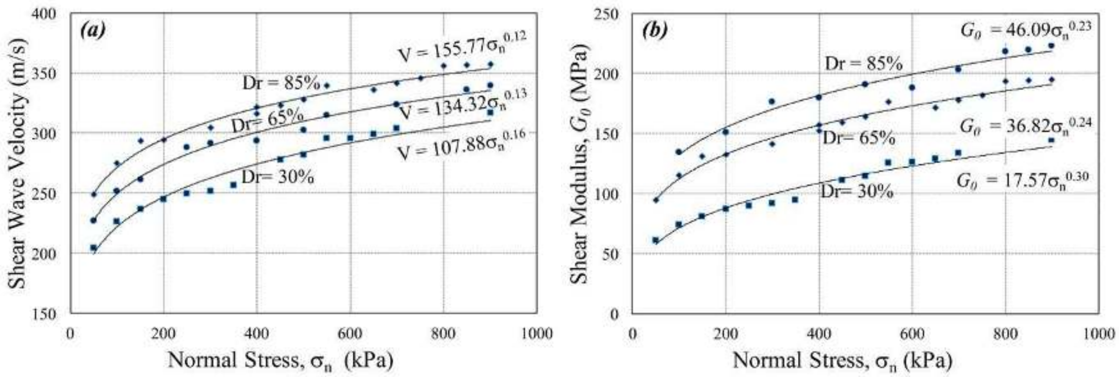

Figure 4. Effect of normal stress and relative density, D_r on: (a) Shear wave velocity, (b) shear modulus of Firuzkuh sand (131).

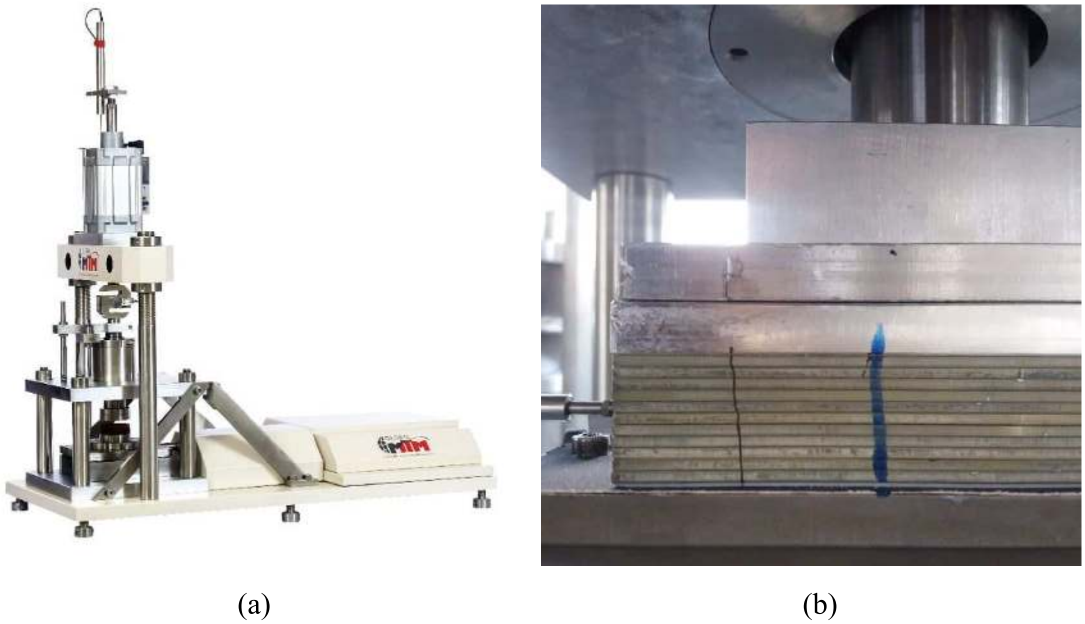

Figure 5. (a) Global MTM Simple shear apparatus, (b) An image of the sample container before shearing.

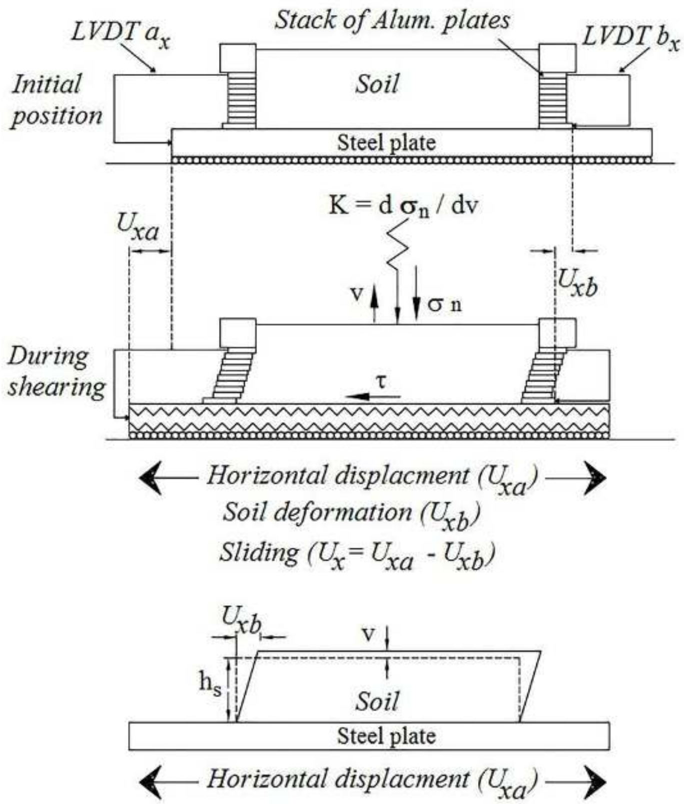

Figure 6. Analogy between the localized shear along pile shaft and a simple shear test with an imposed normal stiffness (modified from Fakharian and Evgin 1997; Uesugi and Kishida 1986).

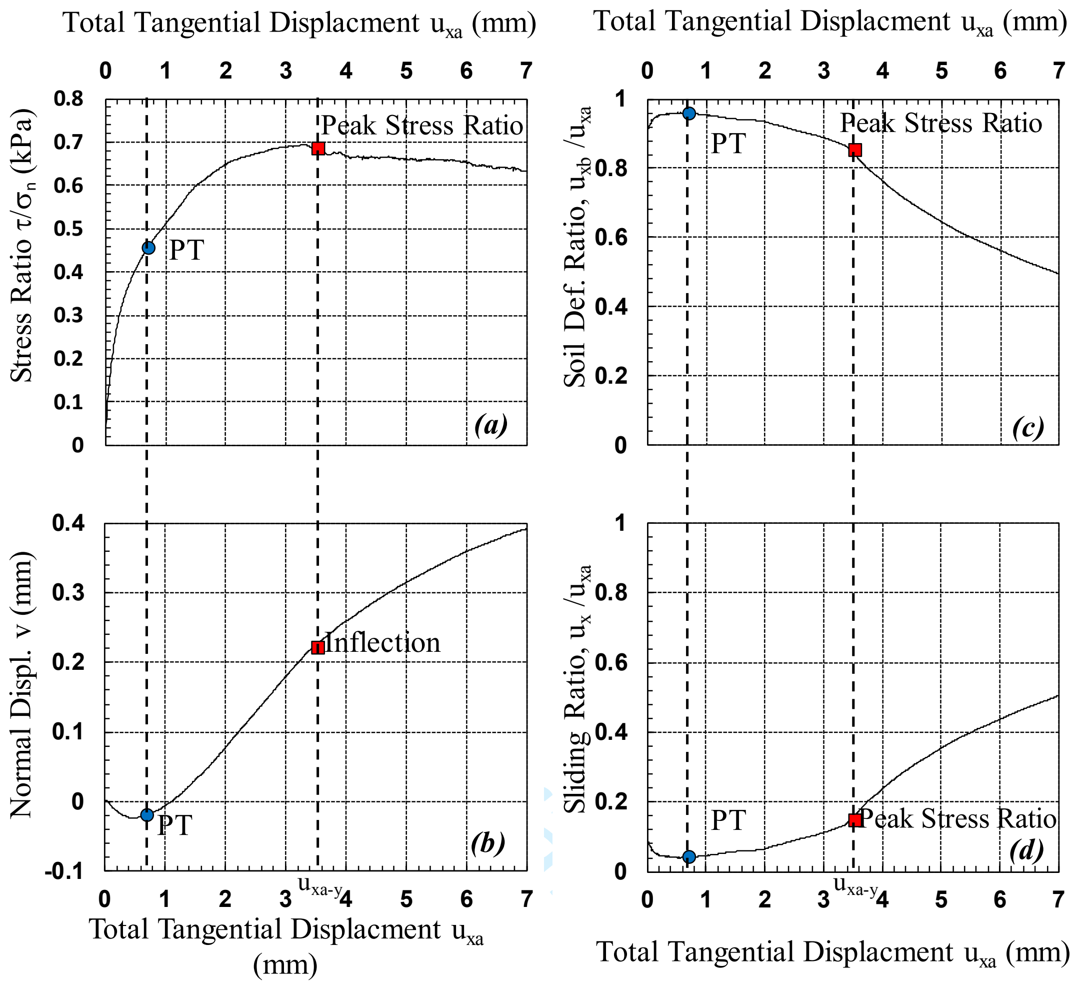

Figure 7. Positions of phase transformation (PT) and inflexion points for MD-100-K400 test.

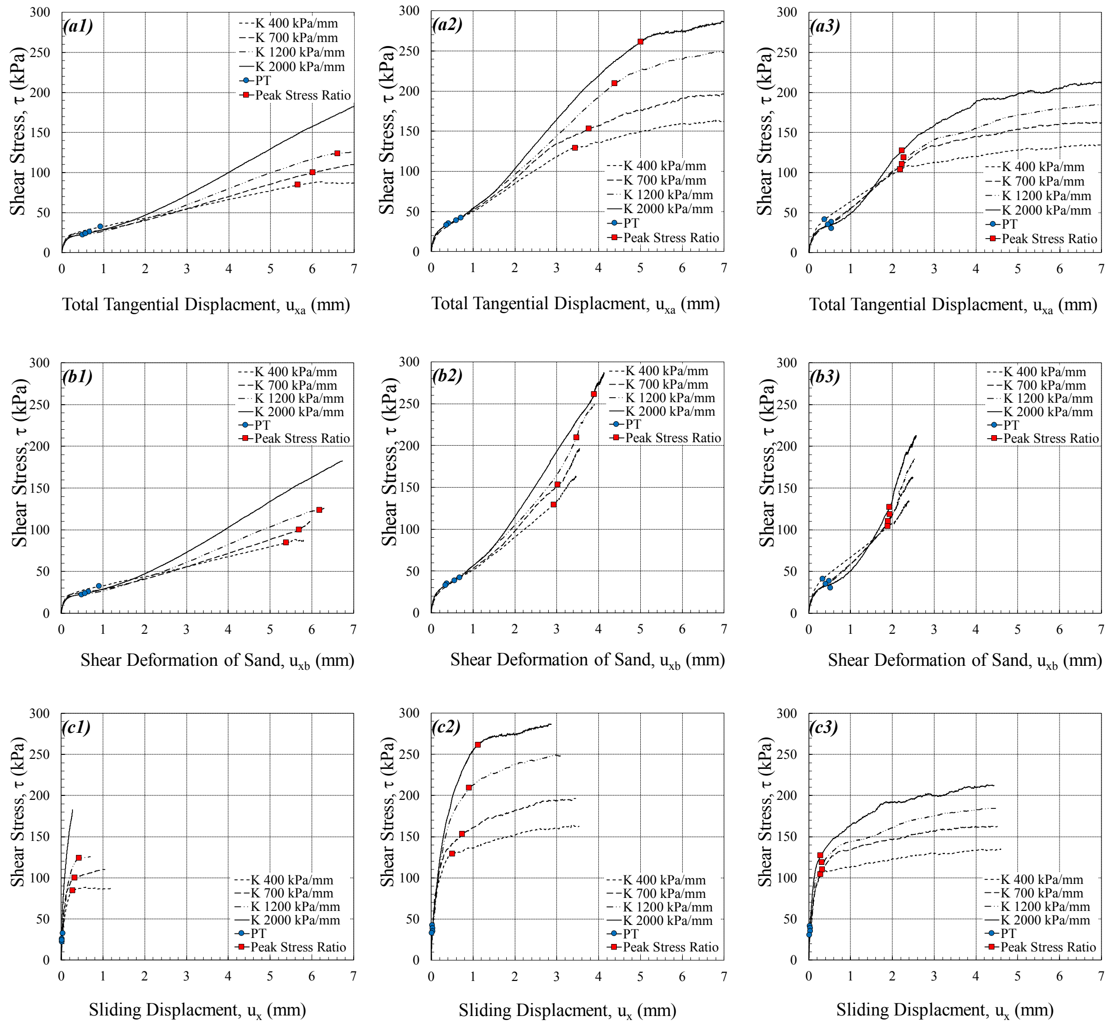

Dr 30% *Dr* 65% *Dr* 85%

Figure 8. Sand-steel interface test results with relative densities 30, 65, 85%, 100 kPa initial normal stress, and 400, 700, 1200, 2000 kPa/mm constant normal stiffness.

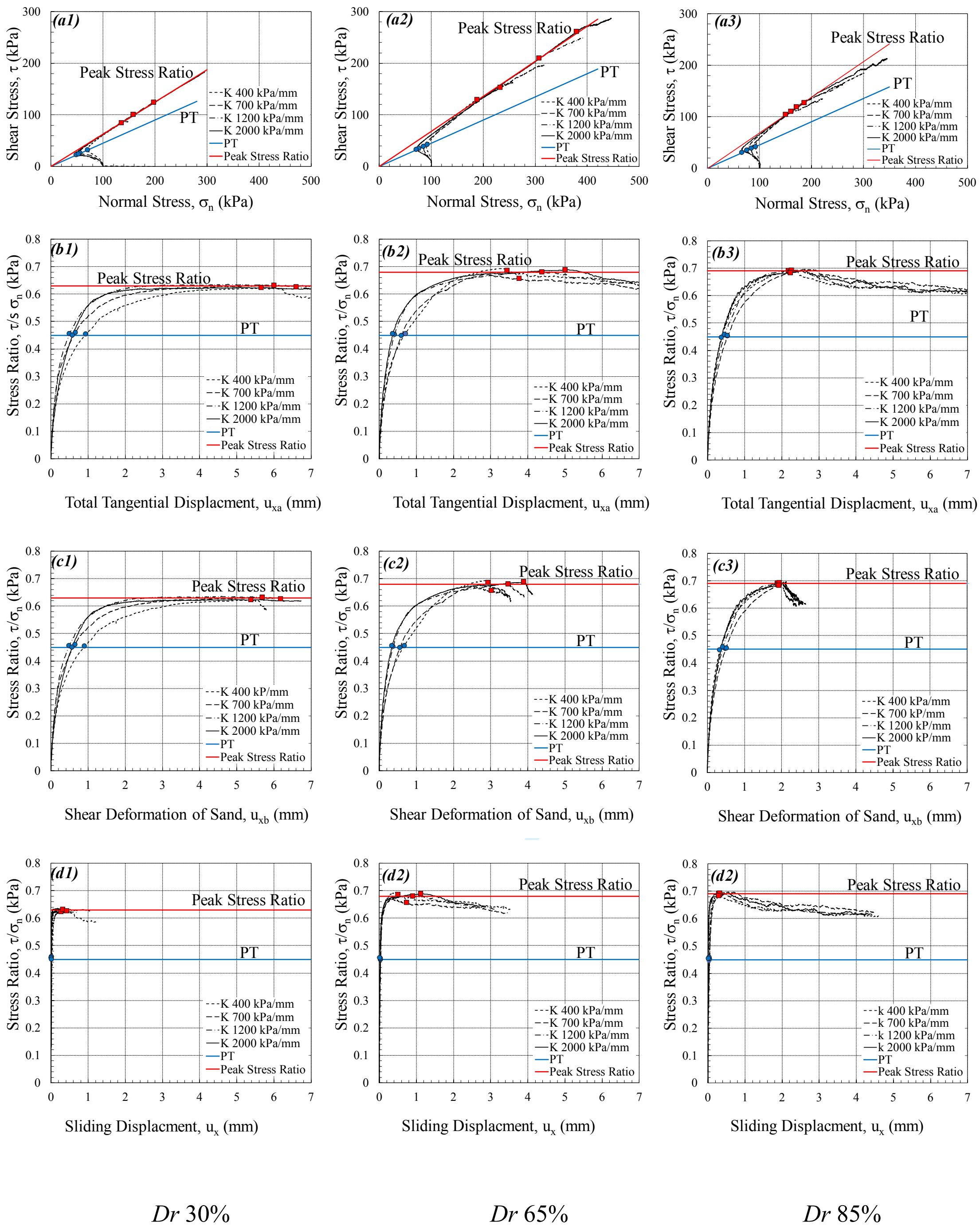

Figure 9. Locations of PT and peak stress ratio points at stress space (a1-a3), stress ratio-total tangential displacement (b1-b3), stress ratio-shear deformation (c1-c3) and stress ratio-sliding displacement (d1-d3) for different relative density and *K* values.

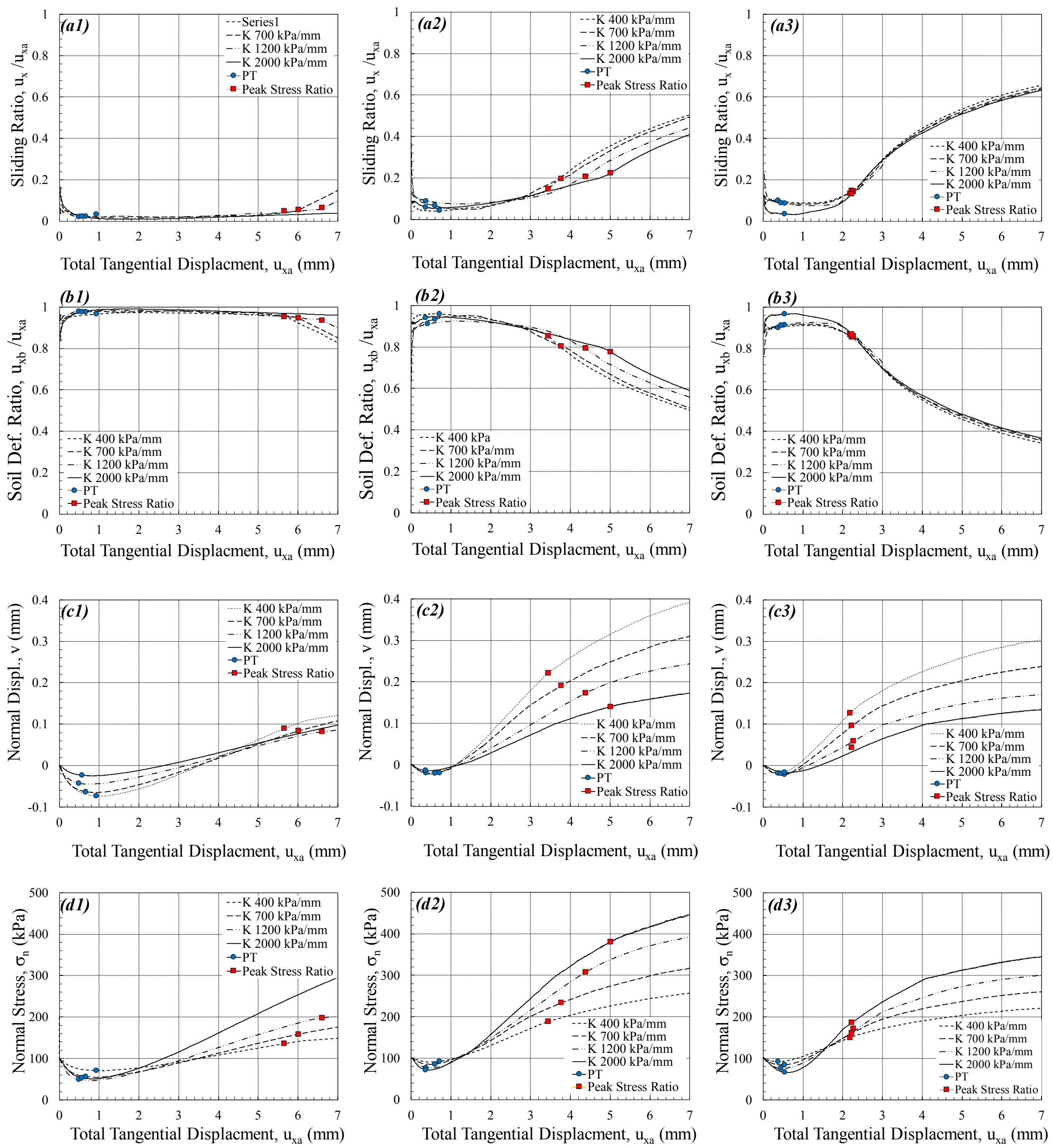

Dr 30% *Dr* 65% *Dr* 85%

Figure 10. More details of the sand-steel interface test results with relative densities 30, 65, 85%, 100 kPa initial normal stress, and 400, 700, 1200, 2000 kPa/mm constant normal stiffness.

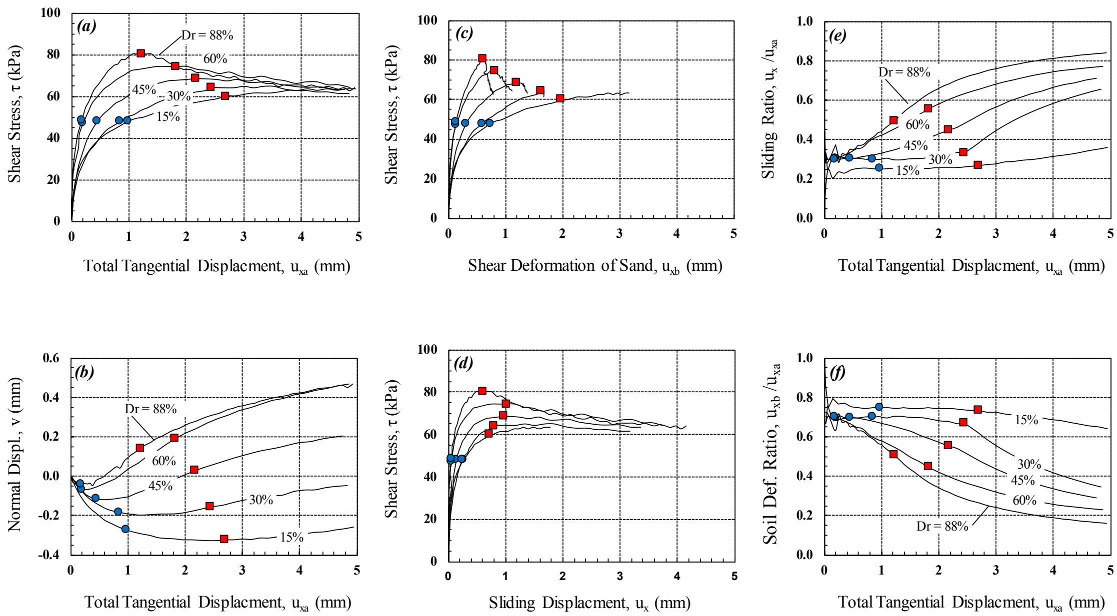

Figure 11. Comparisons between the results of CNL sand-steel interface tests with initial relative densities 15, 30, 45, 60 and 88% and initial normal load of 100 kPa (with surface roughness of 25 μm) (Fakharian 1996).

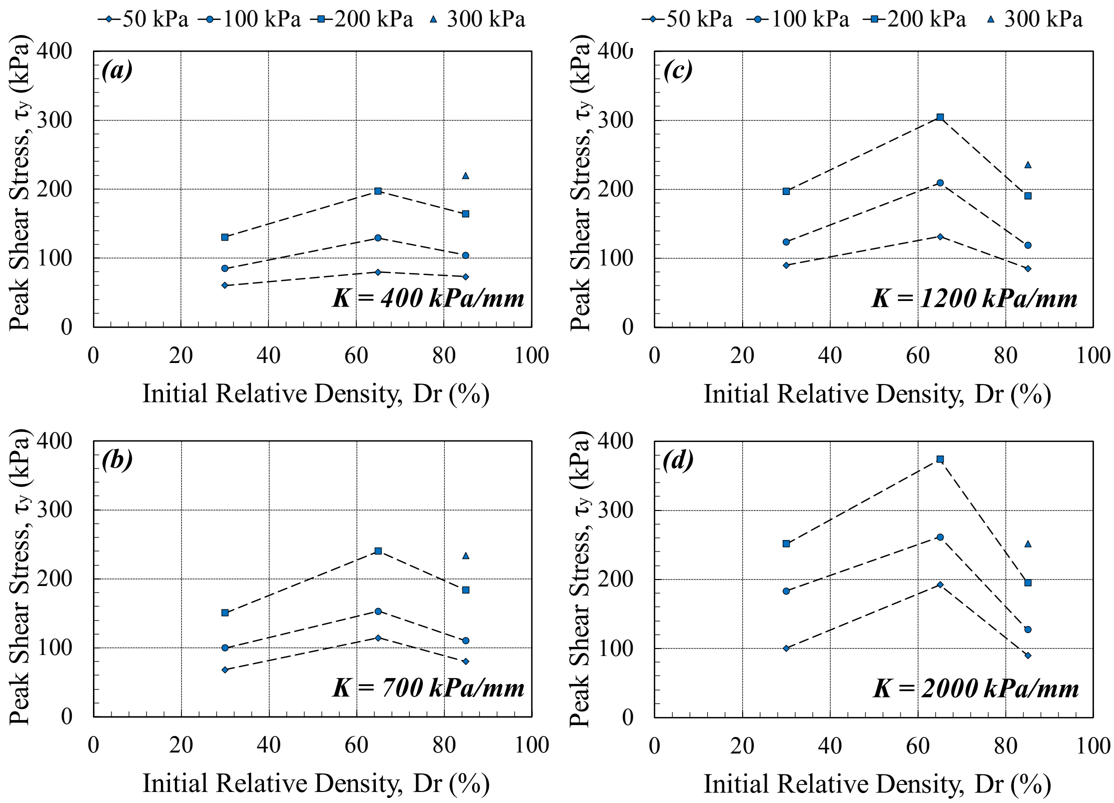

Figure 12. Peak shear stress, τ_y varaition with relative density, for normal stifnesses of 400, 700, 1200 and 2000 kPa/mm.

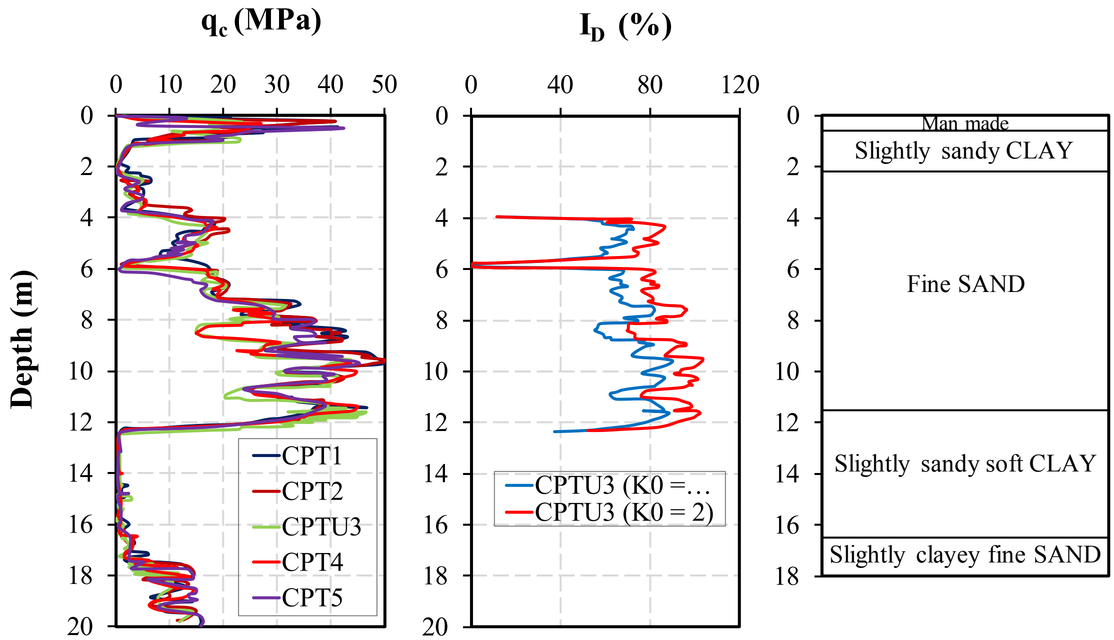

Figure 13. Soil layering, CPT and density index profiles at Loon-Plage (modified from Benzaria et al. 2013).

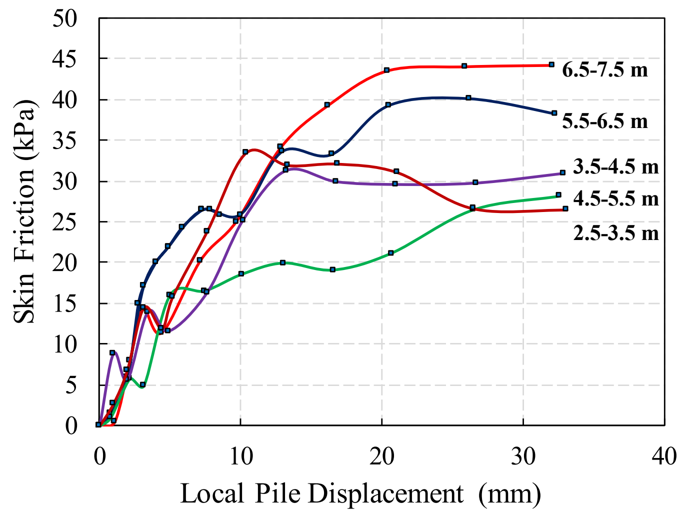

Figure 14. Local shear transfer (t-z) curves in Flanders sand from static load test on CFA pile F4 at different depths (modified from Benzaria et al. 2013).

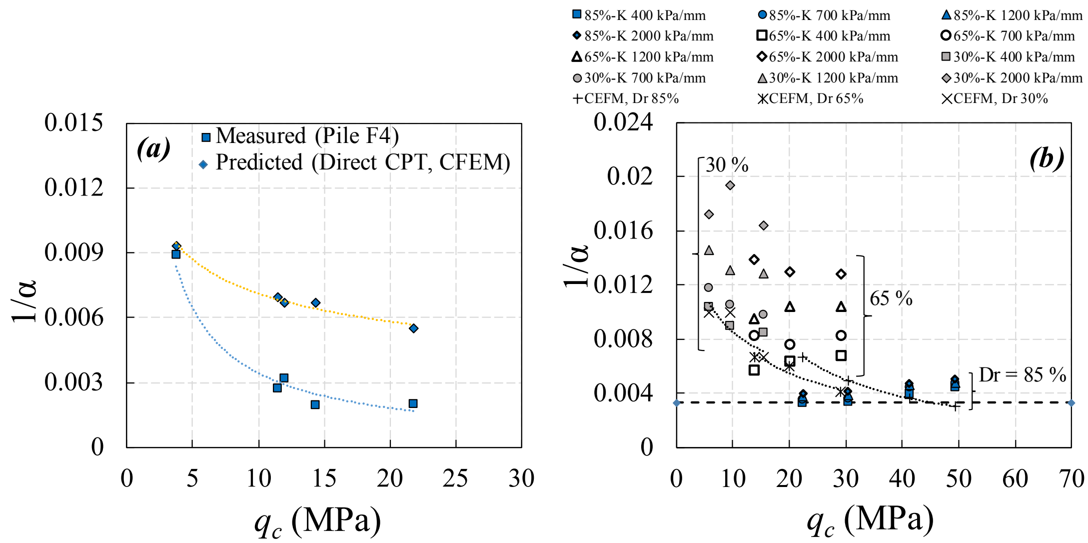

Figure 15. Magnitudes of 1/α for: (a) peak shear strength obtained from deduced t-z curves and proposed values of CFEM for Pile F4, and (b) peak stress ratio for sand-steel interface tests and proposed values of CFEM for 30, 65 and 85% relative densities.

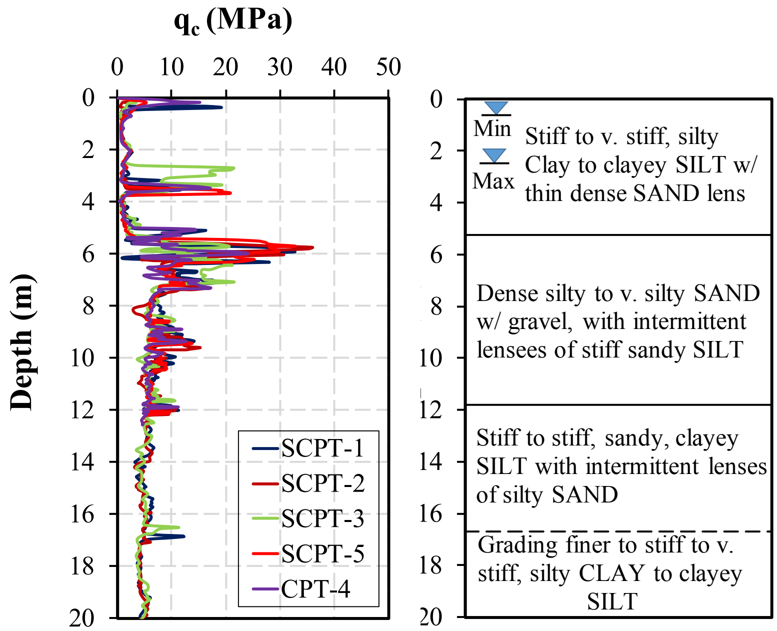

Figure 16. Soil layering and CPT profiles at GEFRS site (modified from Li et al. 2017).

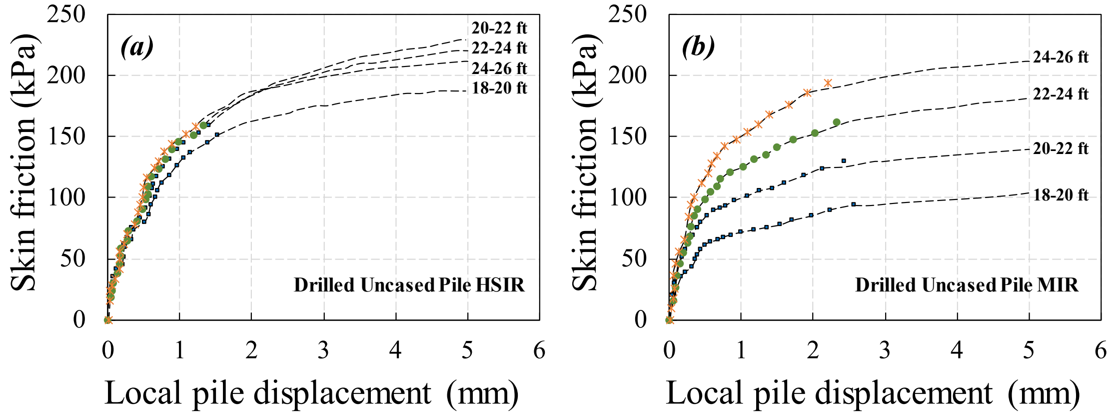

Figure 17. Measured, fitted and proposed t-z responses for the two uncased test piles (a) HSIR and (b) MIR for load increments between 5.5 to 7.9 m (18–26 ft) (Li et al. 2017).

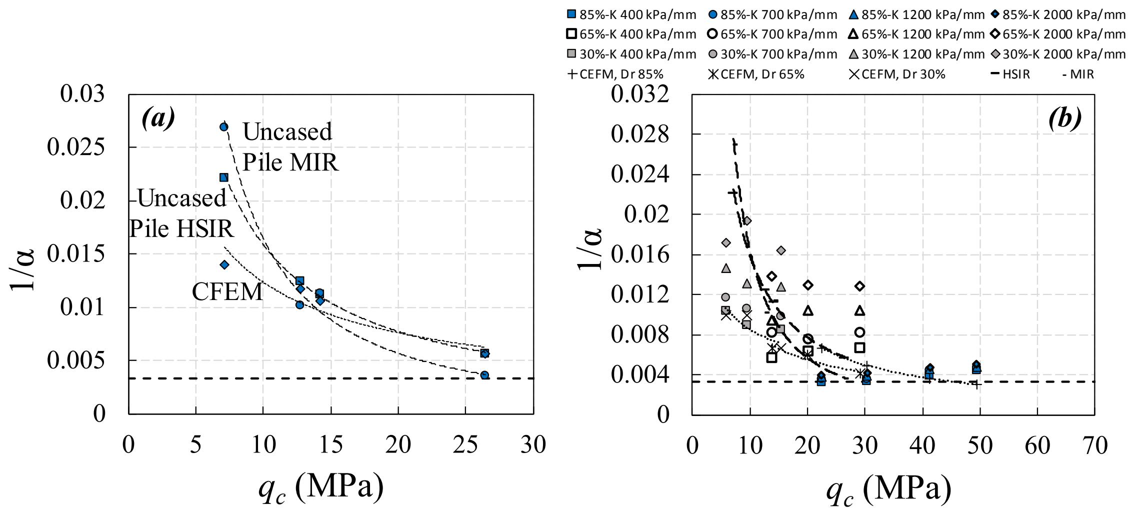

Figure 18. Magnitudes of 1/α for: (a) mesured values obtained from deduced t-z curves and proposed values of CFEM for Piles MIR and HSIR, and (b) comparing peak stress ratio for sand-steel interface tests and obtained values for Piles MIR and HSIR.